PORTIONS OF THIS DOCUMENT ARE ILLEGIBLE

C00-3056-41

MASTER

There is no objection from the patent point of view to the publication or dissemination of the document(s) listed in this letter.

BROOKHAVEN PATENT GROUP

9/24 1979 By [signature]

Thermo Electron CORPORATION

Thermo Electron
CORPORATION

Report No. TE4258/4247-2-80

# DOE/JPL ADVANCED THERMIONIC TECHNOLOGY PROGRAM

## PROGRESS REPORT NO. 39

## APRIL - MAY - JUNE 1979



DOE Contract EY-76-C-02-3056
JPL Contract 955009

Prepared by

Thermo Electron Corporation
101 First Avenue
Waltham, Massachusetts 02154

lb

BLANK PAGE

Thermo Electron CORPORATION

CONTENTS

INTRODUCTION

PART ONE: DOE TASKS

I. SURFACE AND PLASMA INVESTIGATIONS
   A. Surface Characterization Chamber Experiments
   B. Spectroscopic Plasma Experiments
   C. Converter Theory
      1. Simplified Analysis of Particle Thermionic Converters
      2. Evaluation of the Effect of Electron Neutral Elastic Collision Cross Section to the Converter Performance

II. LOW-TEMPERATURE CONVERTER DEVELOPMENT
   A. Converter No. 207: Tungsten Emitter, Tungsten Oxide Collector
   B. Converter No. 215, Heat Flux

III. COMPONENT HARDWARE DEVELOPMENT
   A. Alloy Hot Shell Development
   B. CVD Hot Shell-Emitter Development

IV. SYSTEM STUDIES

V. TAM MODULE DEVELOPMENT
   A. Converter No. 218: CVD Silicon Carbide Converter No. 1
   B. Converter No. 221: CVD Silicon Carbide Converter No. 2

## PART TWO: JPL TASKS

I. HIGH-TEMPERATURE CONVERTER EVALUATION
   A. Converter No. 216: Tungsten Emitter, Molybdenum Oxide Collector
   B. JPL Converter No. 7: Zr-O-W(100) Emitter, Nobium Collector

II. ADVANCED CONVERTER STUDIES
   A. Noncesiated Particle Thermionic Converter Test
   B. Cesiated Particle Thermionic Converter Test

III. POSTOPERATIONAL DIAGNOSTICS

IV. CYLINDRICAL CONVERTER COMPONENT DEVELOPMENT

V. CORRELATION OF DESIGN INTERFACES

# INTRODUCTION

During the week of June 4, Thermo Electron personnel presented the following papers at the International Conference on Plasma Science held in Montreal:

"Thermionic Converters with Metal Oxide Collectors," D.B. Goodale, M. Saunders, and D. Lieb, IEEE Plasma Science Conf. Record-Abs., Paper No. 6D3 (Work performed under DOE Contract No. EY-76-C-02-3056 and JPL Contract No. 955009).

"Simplified Analysis of Particle Thermionic Converters," C.C. Wang, IEEE Plasma Science Conf. Record-Abs., Paper No. 6D4 (Work performed under DOE Contract No. EY-76-C-02-3056).

"Particle Thermionic Converter Experiments," P.E. Oettinger, G. Stark, and F.N. Huffman, IEEE Plasma Science Conf. Record-Abs., Paper No. 6D5 (Work performed under DOE Contract No. EY-76-C-02-3056).

"Investigations of a Pulsed Triode Thermionic Converter," C. Lee and P.E. Oettinger, IEEE Plasma Science Conf. Record-Abs. Paper No. 6D6 (Work performed under JPL Contract No. 955009).

"Numerical Study of Thermionic Converter Plasmas," C.C. Wang, IEEE Plasma Science Conf. Record-Abs., Paper No. 5B10 (Work performed under DOE Contract No. EY-76-C-02-3056).

"The Thermionic Emitting Properties of Coadsorbed Zirconium and Oxygen on the W(110) Crystal Face," L.R. Danielson and L.W. Swanson, IEEE Plasma Science Conf. Record-Abs., Paper No. 6D1 (Work performed at Oregon Graduate Center).

The DOE-NASA Thermionic Contractors Program Review was held in conjunction with this conference. Thermo Electron reviewed its program(1) on June 6. In addition, Thermo Electron personnel participated in the associated Plasma, Electrode and Space System Workshops.

Drs. C.N. Manikopoulos and William Lee of Rutgers University visited Thermo Electron on May 3. Plasma and surface physics problems were discussed.

Dr. Lynwood Swanson of the Oregon Graduate Center spent May 31 at our laboratories. Electrode characteristics, especially those of lanthanum hexaboride and of W(110)-O-Zr, were reviewed.

Dr. Edmund Storms of the Los Alamos Scientific Laboratory worked June 11 - 13 on lanthanum hexaboride emission, Auger and FERP measurements at Thermo Electron. This effort proved to be beneficial for both parties.

Thermo Electron CORPORATION

# PART ONE: DOE TASKS

## I. SURFACE AND PLASMA INVESTIGATIONS

### A. SURFACE CHARACTERIZATION CHAMBER EXPERIMENTS

The codeposition of cesium and oxygen onto $LaB_{6.5}$ can produce a low work function surface (1.0 eV) as described in the last progress report. The thermal stability of this surface was investigated by measuring the work function, coverages and electron reflectivities as a function of heating temperature. The sample was allowed to cool after the brief heating, and all measurements were made near room temperature. The temperature was measured by an infrared pyrometer using the emissivity of $LaB_{6.5}$ at infrared wavelengths equal to 0.55, as determined by Ircon. The initial work function at room temperature was slightly higher than 1.0 eV due to an overnight wait. The work functions and Auger percent coverages versus heating temperature are shown in Figure 1. The low work function surface is stable to 390 K. After heating to 580 K, two-thirds of the cesium had desorbed, and the work function rose to 2.52 eV Heating to 700 K removed nearly all the cesium, although oxygen was still present. This result indicates that at least some oxygen forms an oxide with the tungsten substrate during heating.

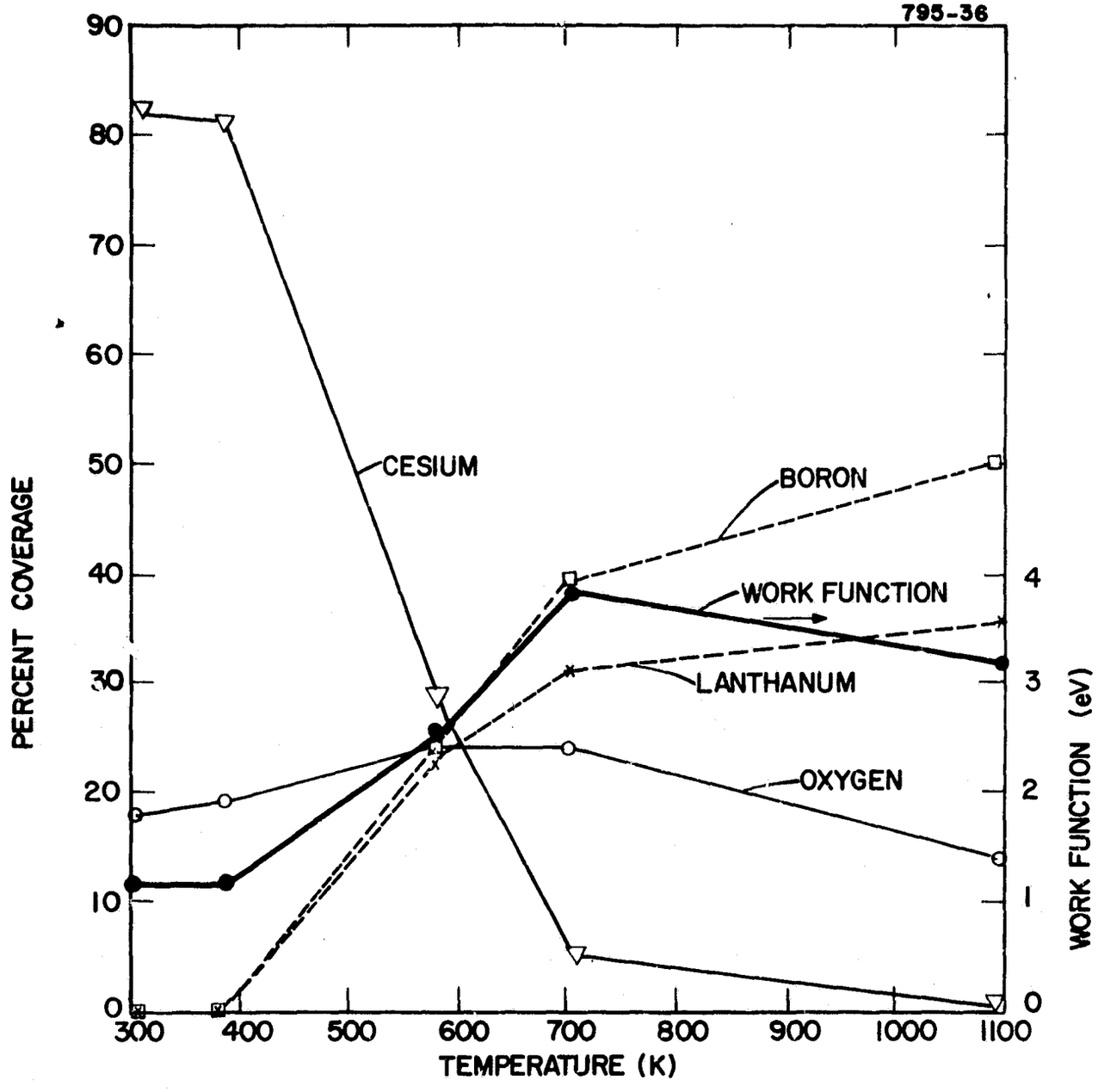


Figure 1. Work Function and Percent Coverages Versus Temperature for Cesium and Oxygen on $LaB_{6.5}$

The reflectivity curves versus heating temperatures are shown in Figure 2. The reflectivity decreases as the cesium coverage decreases and the work function increases. Shifts in the maxima and minima of reflectivity peaks, such as these, can be used to separate the surface and bulk contributions to the work function.(2) Although the data here are not detailed enough to permit accurate separation, the large changes in surface stoichiometry and temperature suggest that both surface and bulk components of the work function are increasing.

The 1.0 eV work functions for iridium and $LaB_{6.5}$ were obtained by simultaneous dosing of cesium and oxygen. An additional experiment was performed with alternating doses of cesium and oxygen. All cesium doses were for 30 seconds with 5 Amps through the cesium channel, and all oxygen doses were $7 \times 10^{-6}$ torr-sec. The reflectivity curves for these alternating doses are shown in Figure 3. The reflectivity increases after each oxygen dose and decreases again after each cesium dose. For runs 2 through 7, the oxygen percent coverage varied between 13 and 17 percent.

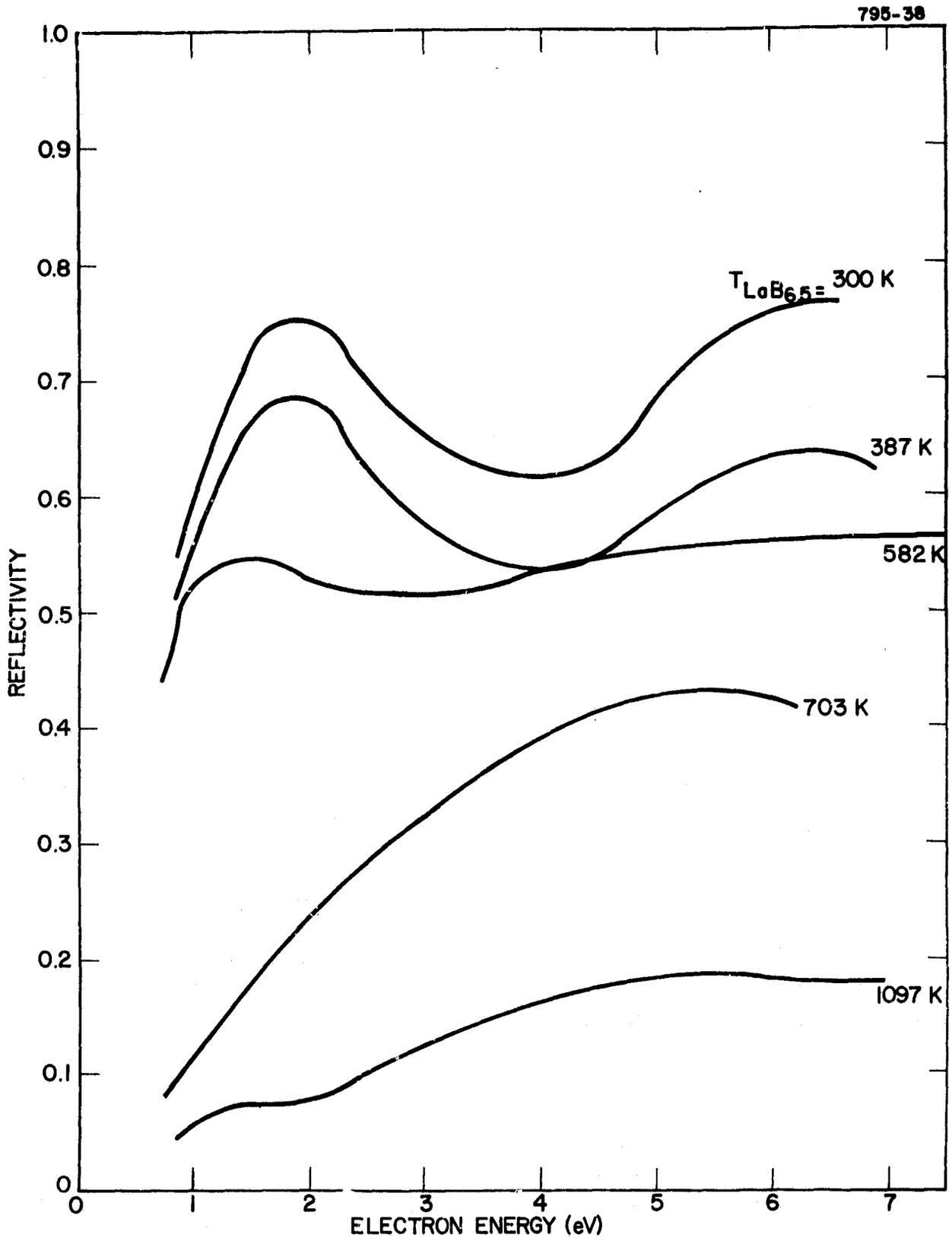


Figure 2. Reflectivity Versus Electron Energy After Heating $LaB_{6.5}$ with Coadsorbed Cesium and Oxygen to the Indicated Temperature

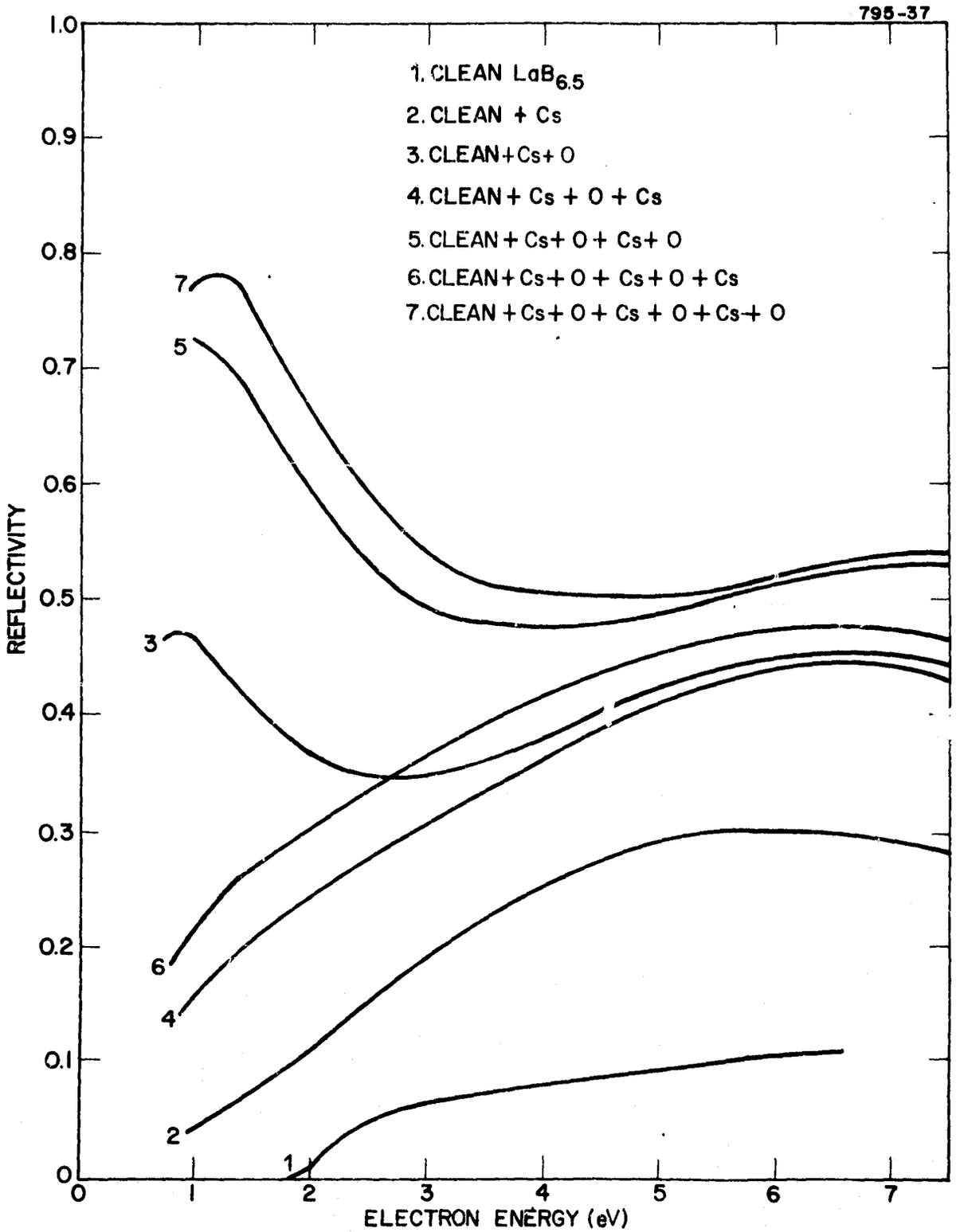


Figure 3. Reflectivity Versus Electron Energy for Alternating Cesium and Oxygen Doses on $LaB_{6.5}$

Thus low reflectivities at threshold can be obtained even with quite large oxygen coverages as long as cesium is deposited last. The low reflectivity surfaces (runs 2, 4, and 6) have work functions of 1.65 to 1.80 eV, whereas the high reflectivity surfaces (runs 3, 5, and 7) have work functions of 2.25 to 2.55 eV. In summary, low electron reflectivities can be obtained for surfaces covered with cesium and oxygen if cesium is deposited last. However, lower work functions do not necessarily imply higher reflectivities.

A comparison of the properties of iridium and $LaB_{6.5}$ surfaces with codeposited cesium and oxygen is given in Table I. These "thick" surfaces have a work function of 1.0 eV, independent of substrate, and reflectivities of about 0.5. In addition, the cesium and oxygen coverages are compatible.

B. SPECTROSCOPIC PLASMA EXPERIMENTS

As part of the plasma investigations, xenon and oxygen gases were added to the hybrid converter (Converter No. 202). After xenon was added, spectroscopic measurements always confirmed the existence of the xenon in the converter under pulsed condition.

TABLE I

SUMMARY OF IRIDIUM AND LANTHANUM HEXABORIDE DATA

| | Ir | | | $LaB_{6.5}$ | | |
|---|---|---|---|---|---|---|
| | Initial Surface | Cs | Cs+O | Initial Surface | Cs | Cs+O |
| Work function | 5.03 eV | 1.6 eV | 1.0 eV | 3.26 eV | 1.82 eV | 1.04 eV |
| Reflectivity at Threshold | - | 0.16 | 0.5 | - | 0.08 | 0.4 |
| Surface Coverages* | | | | | | |
| $Cs_{563}$ | 3% | 19% | 80% | - | 9% | 81% |
| $O_{510}$ | 1% | 1% | 14% | 1% | 2% | 19% |
| $Ir_{1908}$ | 87% | 69% | 6% | - | - | - |
| $B_{179}$ | - | - | - | 74% | 62% | - |
| $La_{625}$ | - | - | - | 25% | 24% | - |
| $C_{273}$ | 6% | 8% | - | 0.2% | 3% | - |
| $N_{380}$ | 3% | 3% | - | - | - | - |

*Subscripts on elements denote energy of Auger peak used to calculate coverages.

However, spectroscopic data showed no sign of oxygen after its addition to the converter. Apparently, oxygen immediately reacts with cesium in the reservoir. After several attempts to introduce oxygen into the converter, the passage between the converter and gasline plugged up. However, the spectrum of the pulsed converter showed dozens of lines that have not been identified. Most of these lines are clustered between 4500 Å and 5400 Å. The relative intensities of these lines are shown in Figure 4. The decay times of these unidentified lines are longer than those of cesium. For example, the decay time of the cesium 4555 Å line is 0.72 ms compared to 0.46 ms for the 4869 Å line, which is not identified. One possible origin of these lines is cesium oxides. Because the reflux gasline was plugged, no additional information could be obtained from this hybrid converter. Therefore, the experiment was terminated and the converter was opened for inspection (see Part Two, Section III).

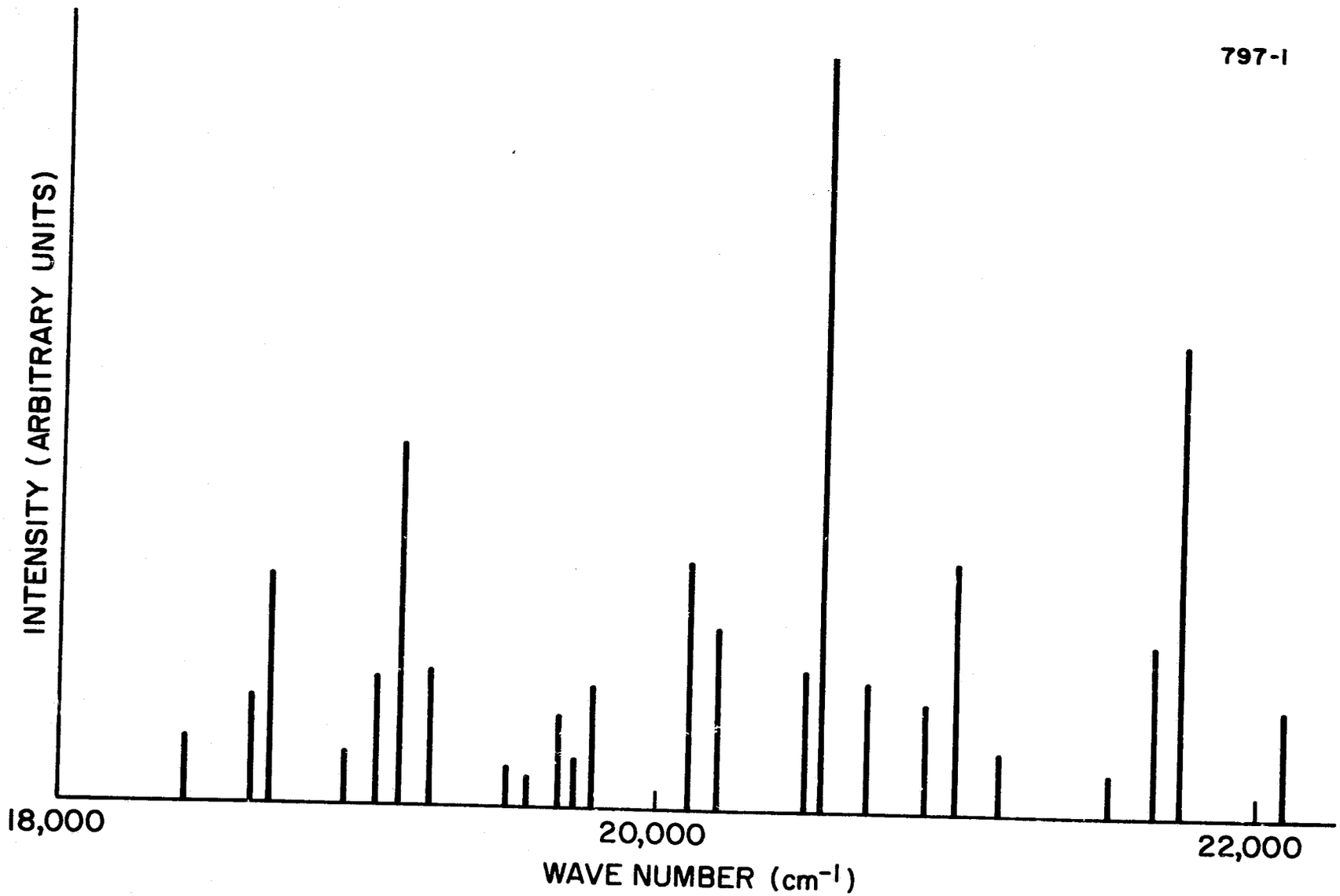


Figure 4. Spectrum of the Unidentified Lines in the Converter

## C. CONVERTER THEORY

### 1. SIMPLIFIED ANALYSIS OF PARTICLE THERMIONIC CONVERTERS

The performance of the particle thermionic converter (PTC) was calculated as a function of particle work function, thermal conductivity, radiation emissivity, and particle dimensions, using a simplified analytical model.(Y3) This model idealizes a particle as a planar electrode.

The work function of barium oxide as a function of temperature can be approximated by(4)

$$\phi = 1.19 + 5 \times 10^{-4} \times T$$

Based on previous Thermo Electron experiments,(5) cesium coverage can reduce the work function of barium oxide up to 0.2 eV. Thus, the cesiated barium oxide work function assumed for these calculations is given by

$$\phi = 0.99 + 5 \times 10^{-4} \times T$$

Bell jar experiments of the PTCs have been operated at electrode temperatures of 1400 K for the emitter and 1073 K for the collector. These temperatures were used as the reference temperatures in the calculations. The thermal conductivity, $\kappa$, of the barium oxide particles was based on information from the Research Center of Purdue University.(6) No data on the radiation emissivity, $\epsilon$, of barium oxide were found. The values assumed varied between 0.05 to 0.4.

The J-V characteristics and efficiencies of multiple electrode converters (i.e., PTCs) as functions of thermal conductivity and thermal emissivity are given in Figures 5 and 6 for the case of bare barium oxide particles. The maximum value of the output current density is 1.9 $A/cm^2$ and the peak efficiency is 11.2% for $\epsilon = 0.05$ and $\kappa = 0.02$. If the work function were reduced by 0.2 eV by cesium, the performance should be greatly improved. Note that the changes of emissivity from 0.005 to 0.4 and thermal conductivity from 0.02 to 0.1 have little effect on the J-V characteristics. However the maximum value of efficiency is reduced from 16.5% to 12% because of the increased heat loss.

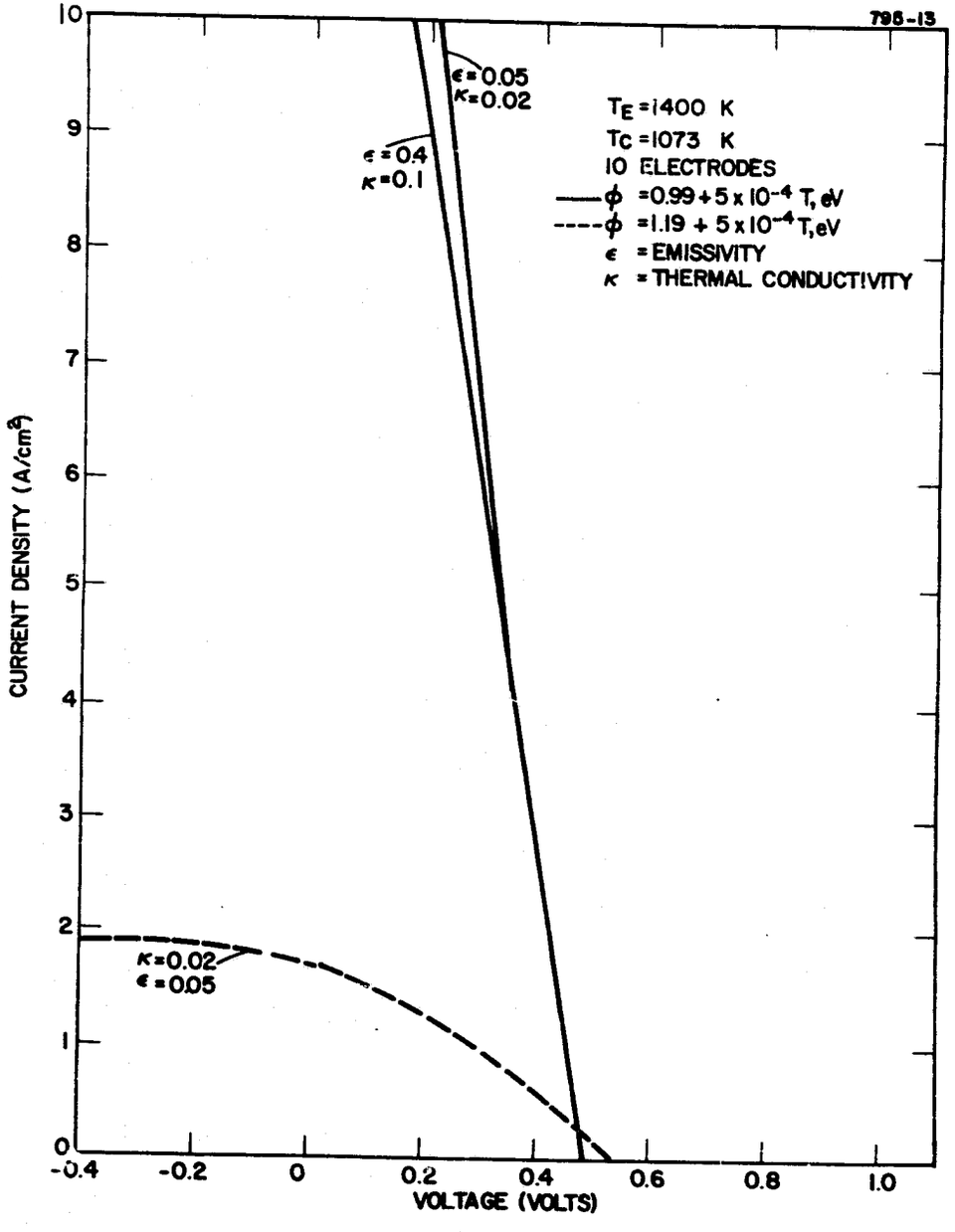


Figure 5. Current Density-Voltage characteristics of a Multiple Electrode Vacuum Converter as a Function of Work Function, Thermal Conductivity and Emissivity.

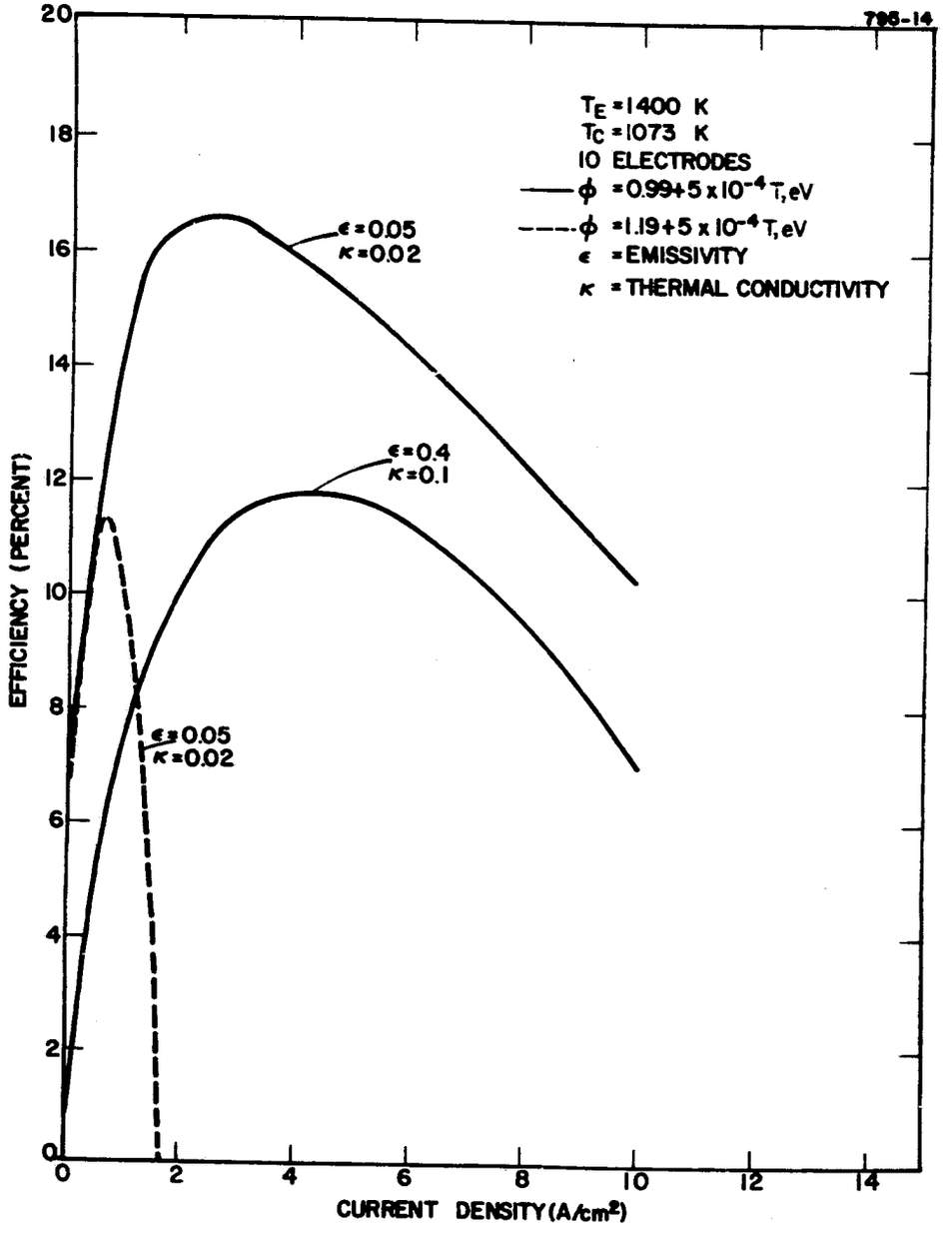


Figure 6. Efficiency of a Multiple Electrode Vacuum Converter as a Function of Work Function, Thermal Conductivity and Emissivity.

The effects of emitter temperature are shown in Figures 7 to 9. As expected, the higher emitter temperature results in better performance. The effects of the number of the electrodes are shown are Figures 10 and 11. The lower number of electrodes offer the better J-V characteristics. However, the converter with six electrodes gives the best efficiency for current densities up to 8 $A/cm^2$. The increased number of electrodes cuts down the heat loss while reducing the output power density.

## 2. EVALUATION OF THE EFFECT OF ELECTRON NEUTRAL ELASTIC COLLISION CROSS SECTION TO THE CONVERTER PERFORMANCE

Dr. Stoenescu has supplied Thermo Electron with the data files and the corresponding interpolation program for calculating the plasma electron transport coefficients. The data files were generated with the best guess electron-neutral elastic collision cross sections and Karule's theoretical cross section. Thermo Electron' plasma program was modified to include Dr. Stoenescu's program and data files. Two sample J-V characteristics were calculated with different plasma electron transport

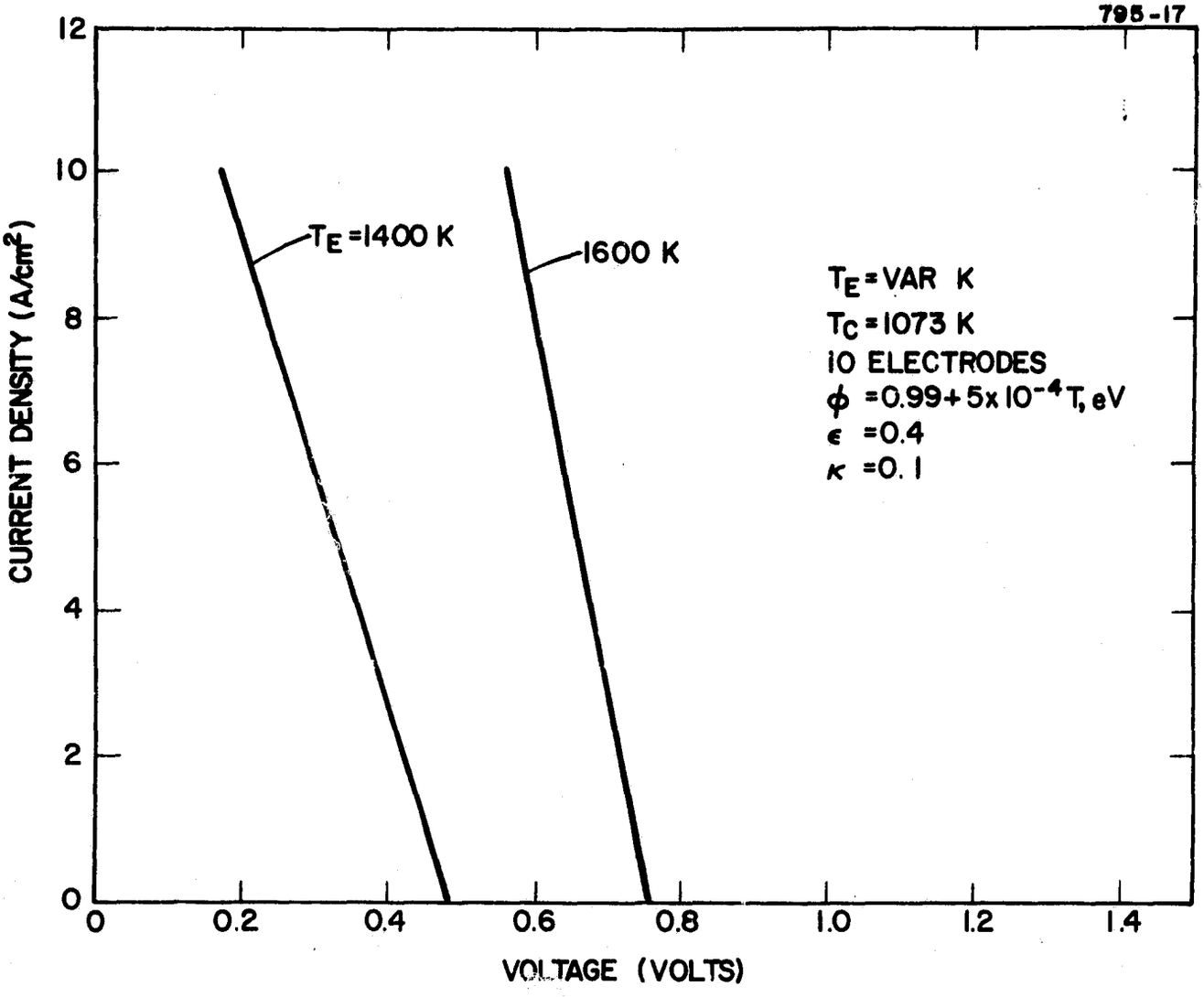


Figure 7. Current Density-Voltage Characteristics of a Multiple Electrode Vacuum Converter as a Function of Emitter Temperature

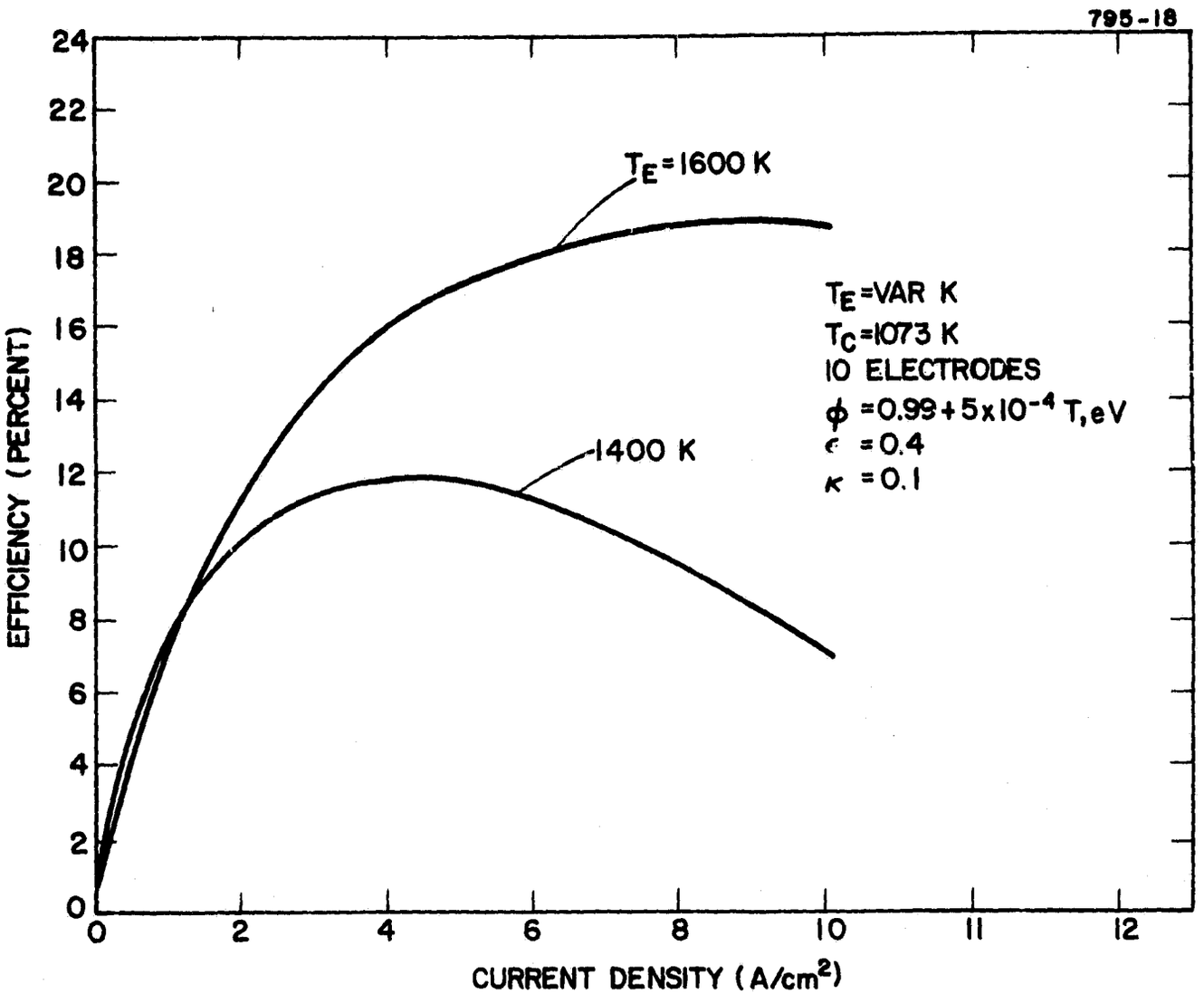


Figure 8. Efficiency of a Multiple Electrode Vacuum Converter as a Function of Emitter Temperature

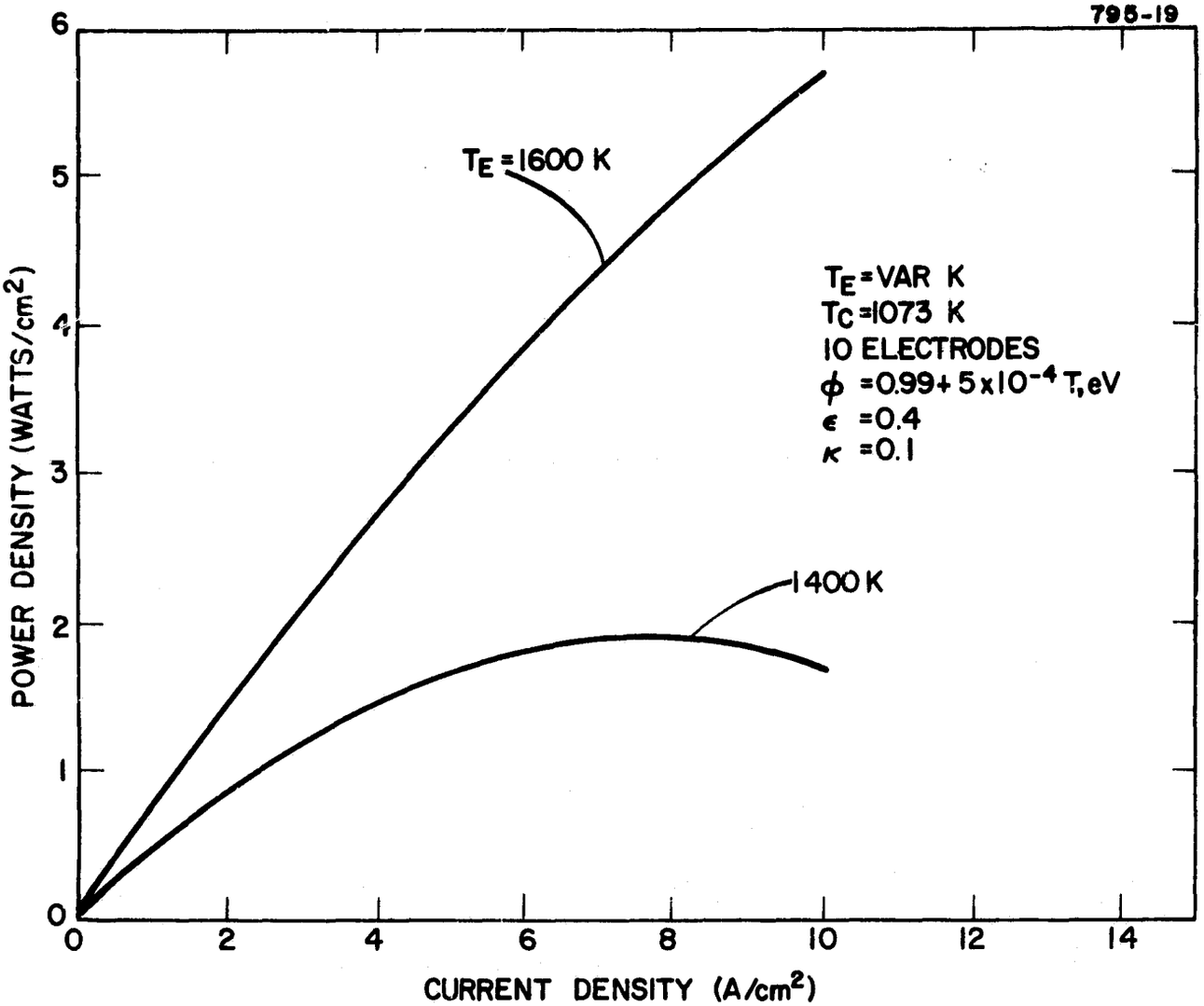


Figure 9. Output Power Density Characteristics of a Multiple Electrode Vacuum Converter as a Function of Emitter Temperature

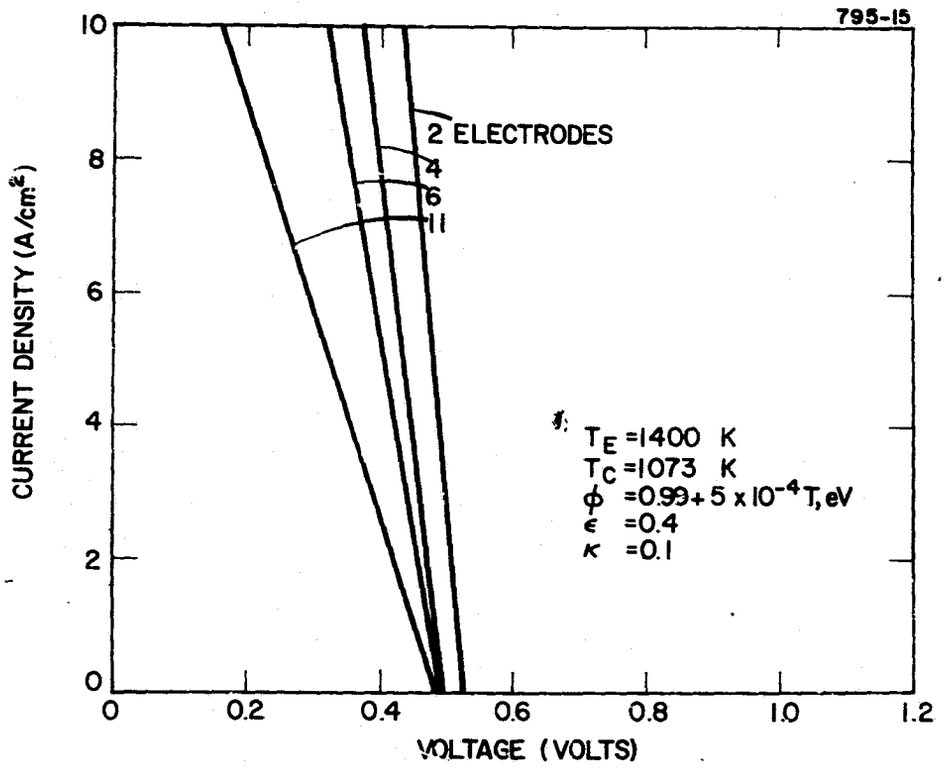


Figure 10. Current Density-Voltage Characteristics of a Multiple Electrode Vacuum Converter as a Function of the Number of Electrodes

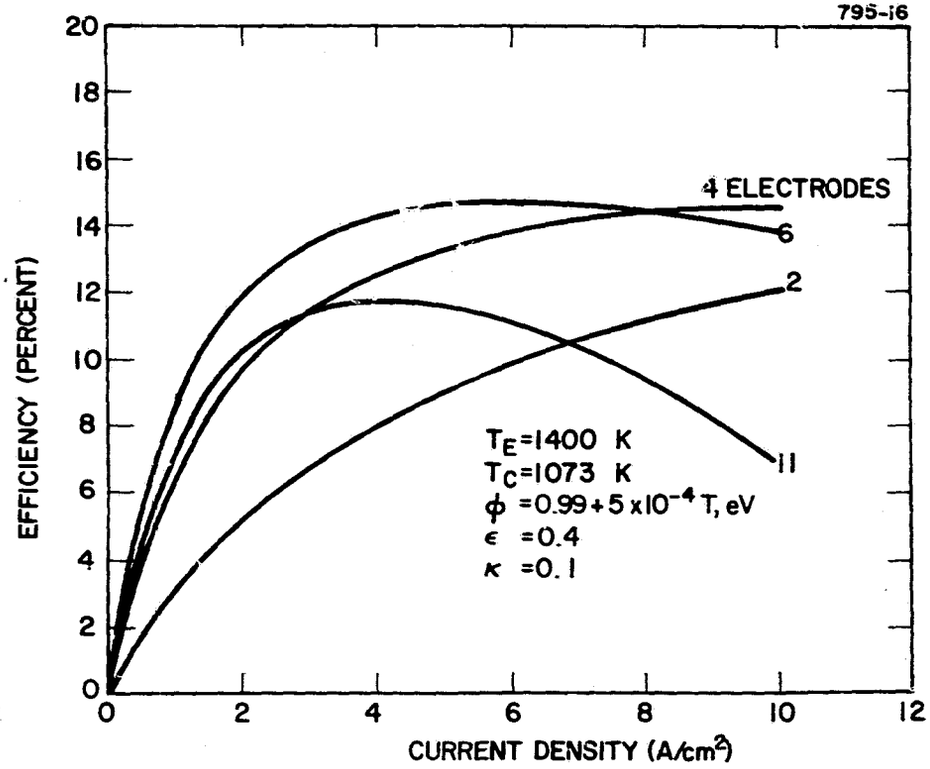


Figure 11. Efficiency of a Multiple Electrode Vacuum Converter as a Function of the Number of Electrodes

coefficients corresponding to the constant cross section approximation, the best guess cross section, and Karule's theoretical cross section. The analytical results for three different sets of transport coefficients are compared with experiment in Figure 12. The spread in the calculated J-V characteristics is split about 0.05 V. Apparently, the constant cross section approximation gives the best comparison with experiment in these particular cases. However, more comparisons must be made before conclusions can be drawn as to the most appropriate cross section.

## II. LOW-TEMPERATURE CONVERTER DEVELOPMENT

### A. CONVERTER NO. 207: TUNGSTEN EMITTER, TUNGSTEN OXIDE COLLECTOR

Performance data for this converter were given in the previous progress report. It continued to exhibit stable "postactivation" performance with a barrier index of 2.12 eV at an emitter temperature of 1400 K. Testing of this diode has been terminated. During the next reporting period, it will be disassembled and a number of postoperational diagnostics (including Auger electron spectroscopy and photomicrographs) will be performed on the collector.

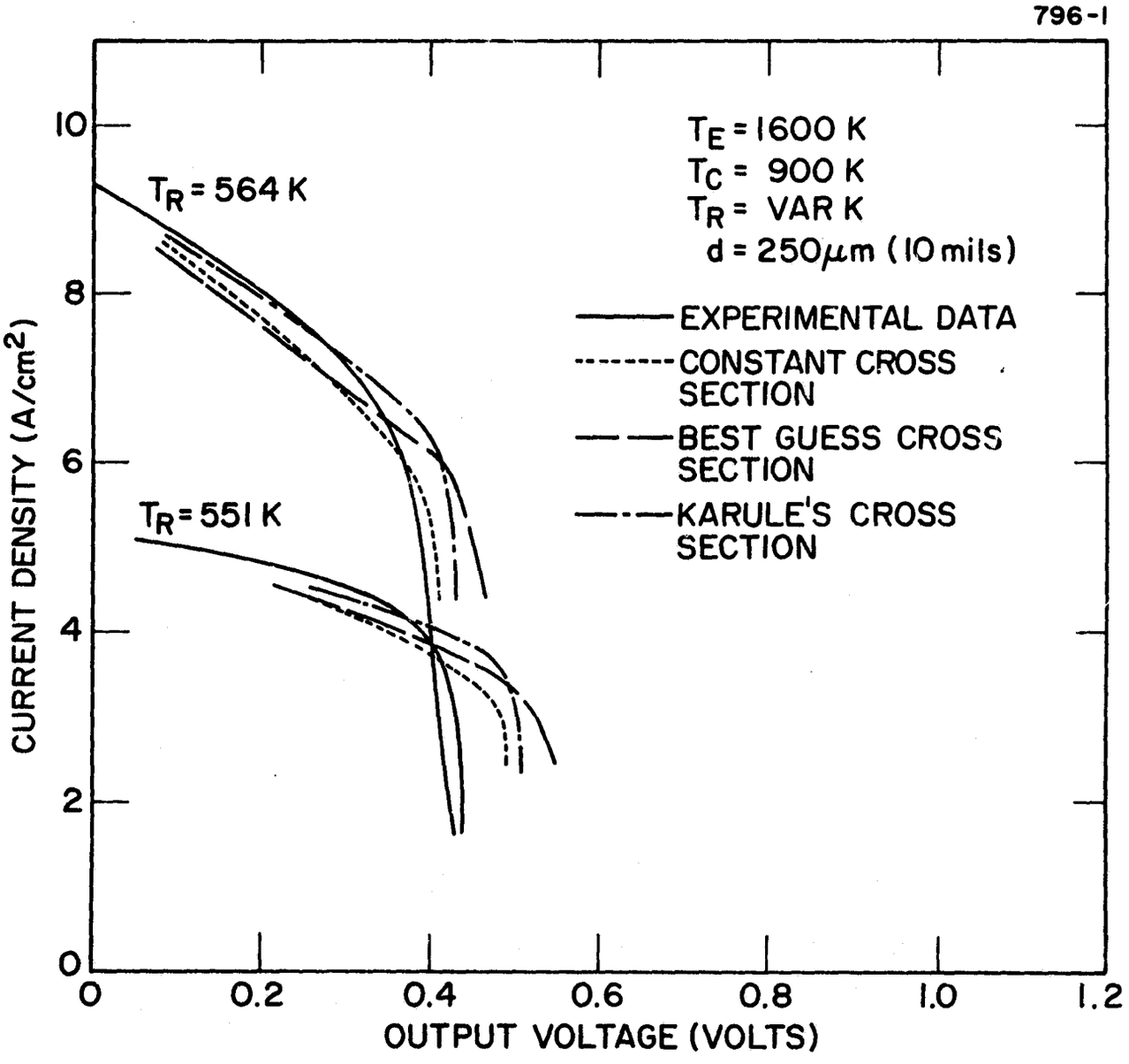


Figure 12. Comparison of Experimental and Theoretical J-V Characteristics

## B. CONVERTER NO. 215, HEAT FLUX: TUNGSTEN EMITTER, NICKEL COLLECTOR

A converter with a polycrystalline tungsten emitter and a 201 nickel collector with a thermally "nulling" auxiliary heater positioned 0.75 mm from the collector surface has been fabricated to facilitate collector heat flux measurements. The design of the heat flux diode is shown in Figure 13, and the block diagram of the experimental arrangement is given in Figure 14.

After carefully outgassing the converter to ensure clean, nonoxygenated electrodes, the diode performance was characterized at emitter temperatures of 1400 K and 1700 K. Cesium families at the two emitter temperatures are shown in Figures 15 and 16. Barrier indicies of 2.12 and 2.16 eV were measured at $T_E$ = 1400 K and 1700 K respectively. The collector work function was measured by the retarding plot method. Collector work function versus $T_C/T_R$ is given in Figure 17. The minimum work function of 1.70 eV corresponds to a $T_C/T_R$ of 1.52.

Heat flux measurements were made in the following manner: the emitter, emitter flange, cesium reservoir, and test stand cooling water temperatures were held to within one degree Kelvin of their set-points by electronic

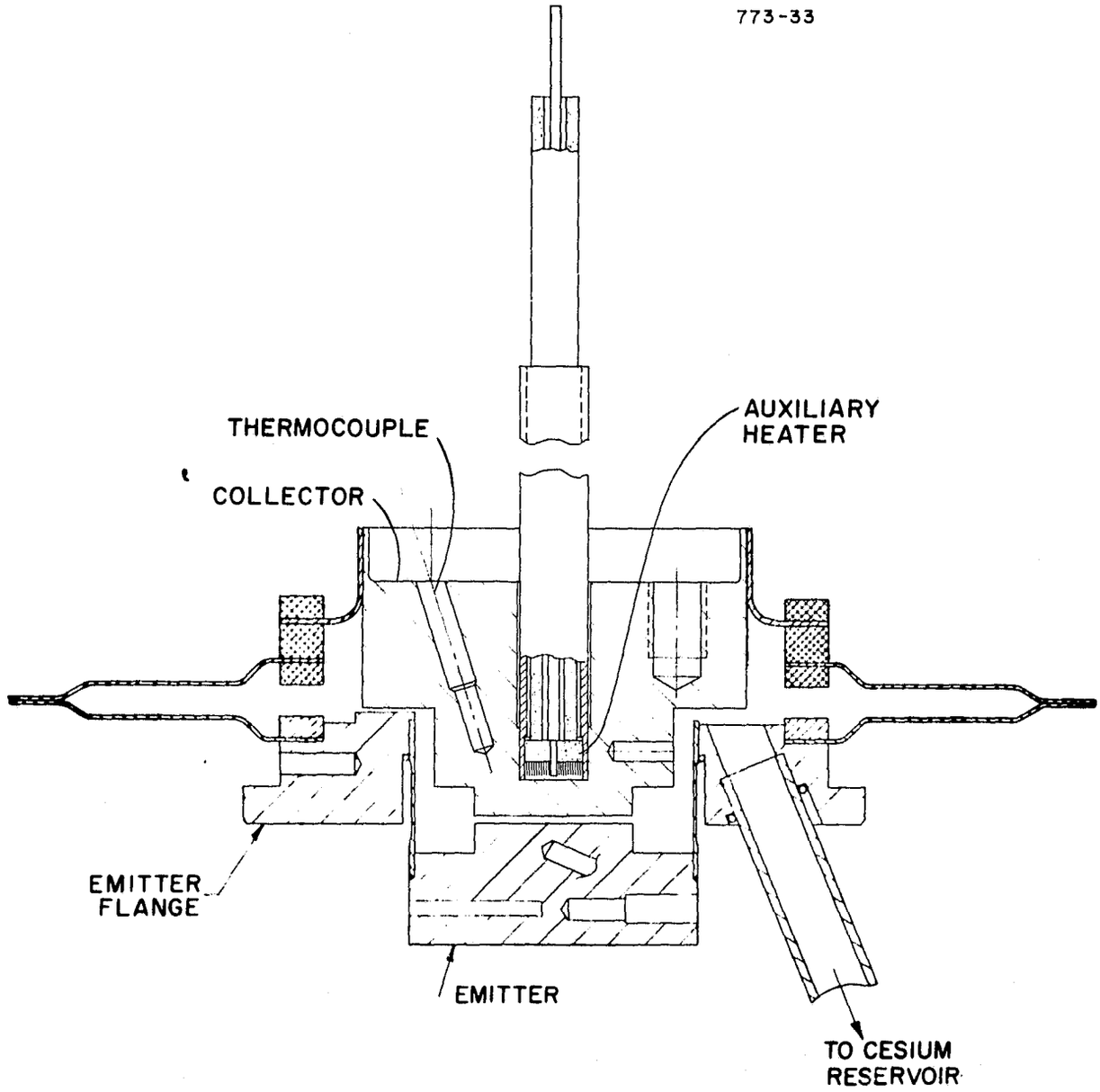


**Figure 13. Heat Flux Diode**

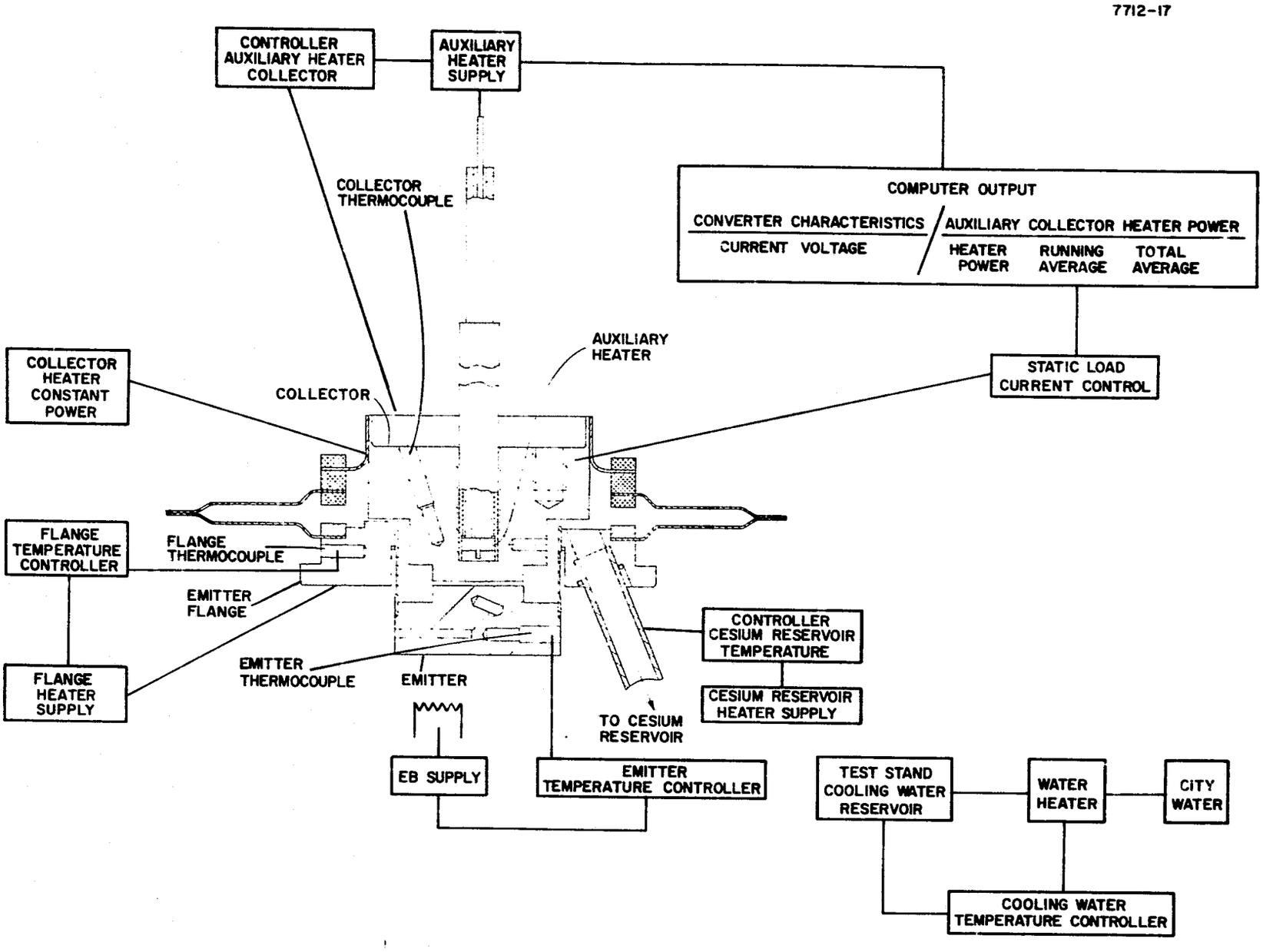


Figure 14. Heat Flux Diode Diagram of Heat Flux Experiment

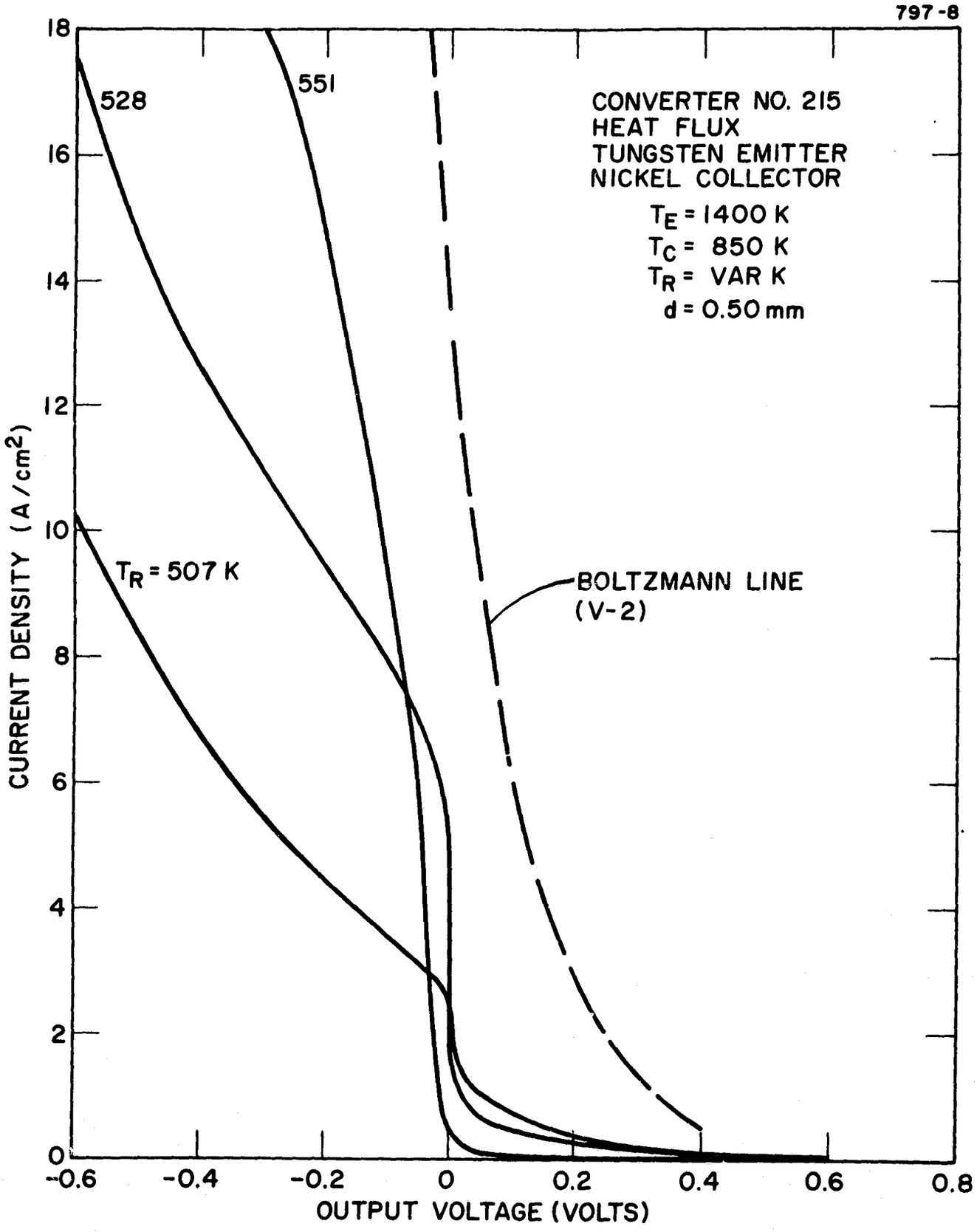


Figure 15. Cesium Family of Converter No. 215 at $T_E$ = 1400 K and $T_C$ = 850 K

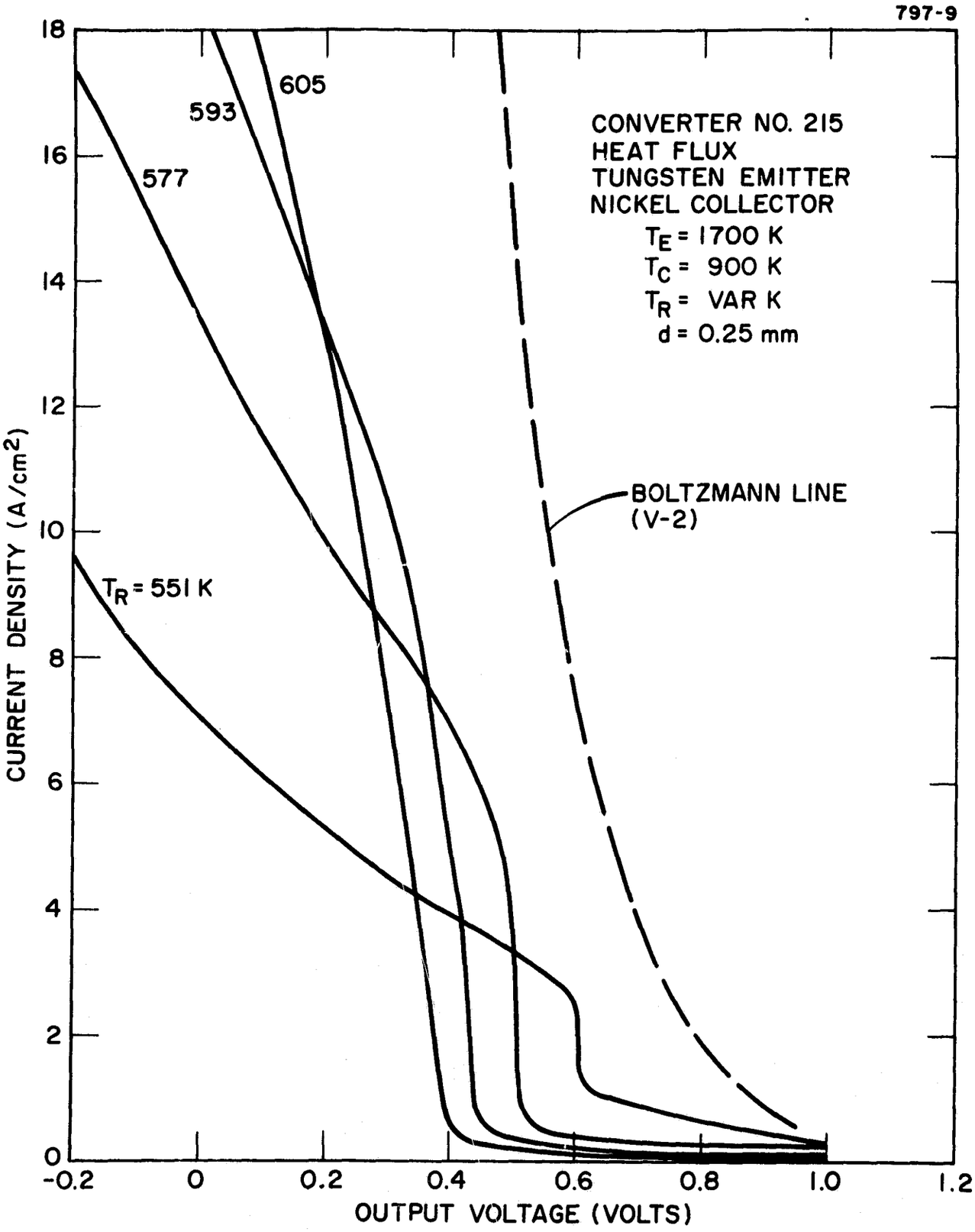


Figure 16. Cesium Family of Converter No. 215 at $T_E$ = 1700 K and $T_C$ = 900 K

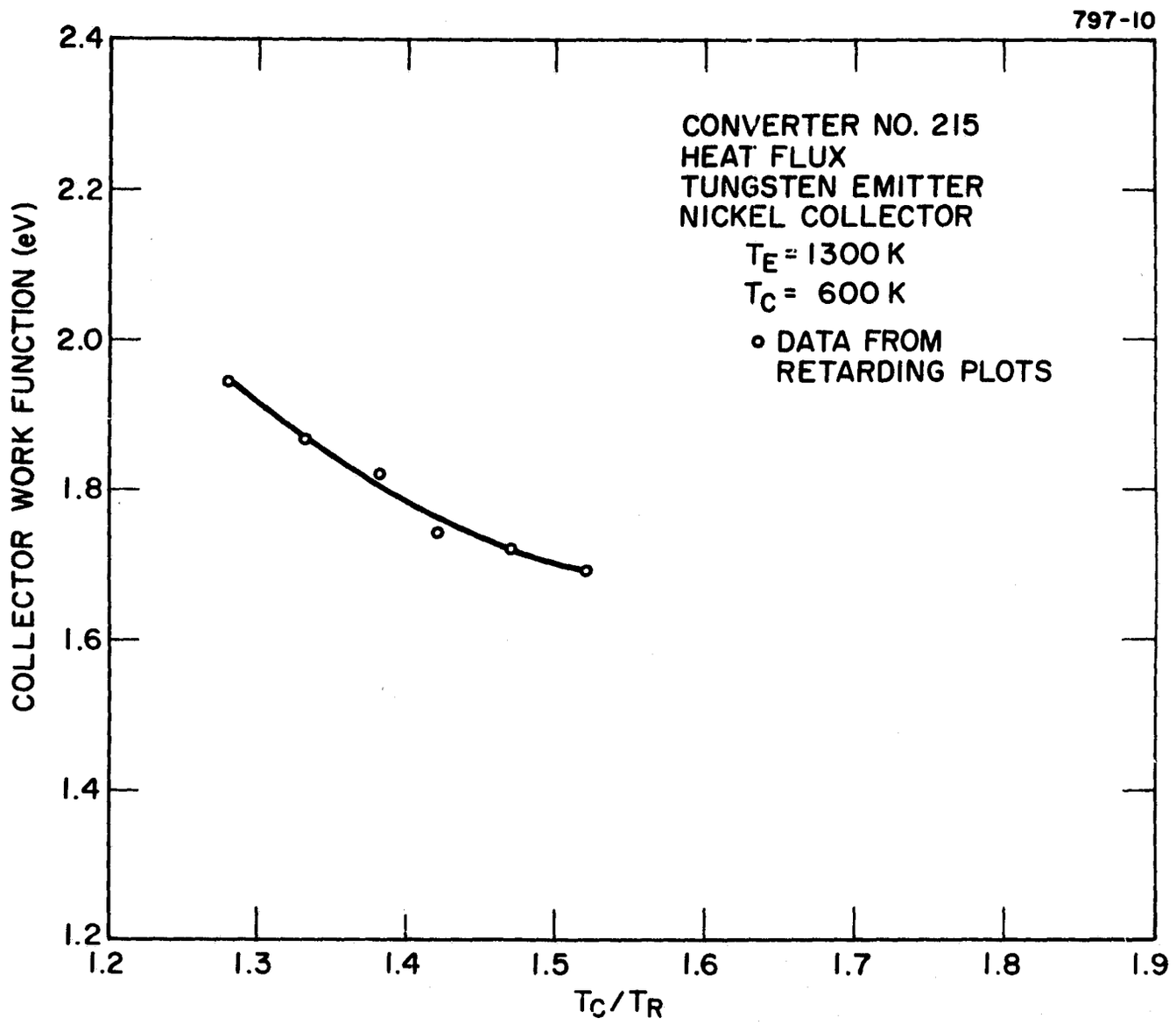


Figure 17. Retarding Plot of Collector Work Function Versus the Ratio of Collector Temperature to Cesium Reservoir Temperature for Converter No. 215

time proportioning temperature controllers. The collector was heated to the desired temperature by a constant power supply and the auxiliary heater. After all converter parameters stablized, the output current was varied incrementally, resulting in different auxiliary heater power requirements. The power to the auxiliary heater is controlled by the computer. Auxiliary heater voltages are measured by taps located as close as possible to the heater element. Auxiliary current was measured by a calibration shunt. These voltages and currents were sampled at five-second intervals by the computer (which calculated the instantaneous heater power, its running average, and its total average). The random error in this power measurement was less than 0.02 watts. After the current was varied, a thermal equilibration time of ten minutes was allowed before data were taken. The auxiliary heater power was then averaged over a ten-minute period in order to minimize fluctuation effects. A least-squares fit was used to determine the straight line slope representing the electron heating of the collector.

Initial heat flux measurements were taken at an emitter temperature of 1400 K, a cesium reservoir temperature of 528 K, an interelectrode spacing of 0.50 mm for various collector temperatures. Current-voltage characteristics, parametric in collector temperature, are given in Figure 18. The operating points at which heat flux determinations were made are indicated on this figure.

The auxiliary heater power versus converter current at a collector temperature of 675 K is given in Figure 19. The heat dissipated in the collector per electron was 2.47 eV at the higher current densities (4 - 9 $A/cm^2$) and 2.51 eV at the lower current densities (0 - 5 $A/cm^2$ This result was reproducible and the data showed little). scatter. The value of the collector work function at these conditions was 1.97 eV (as determined by the retarding plot method).

Figure 20 shows heat flux measurements parametric in collector temperature (see Figure 18 for operating points of the heat flux determinations). Collector temperatures of 850, 750, and 675 K correspond to work functions of 1.70, 1.75, and 1.97 eV, respectively. Heat production at the collector was 2.27 eV for $T_C$ = 850 K; 2.45 eV

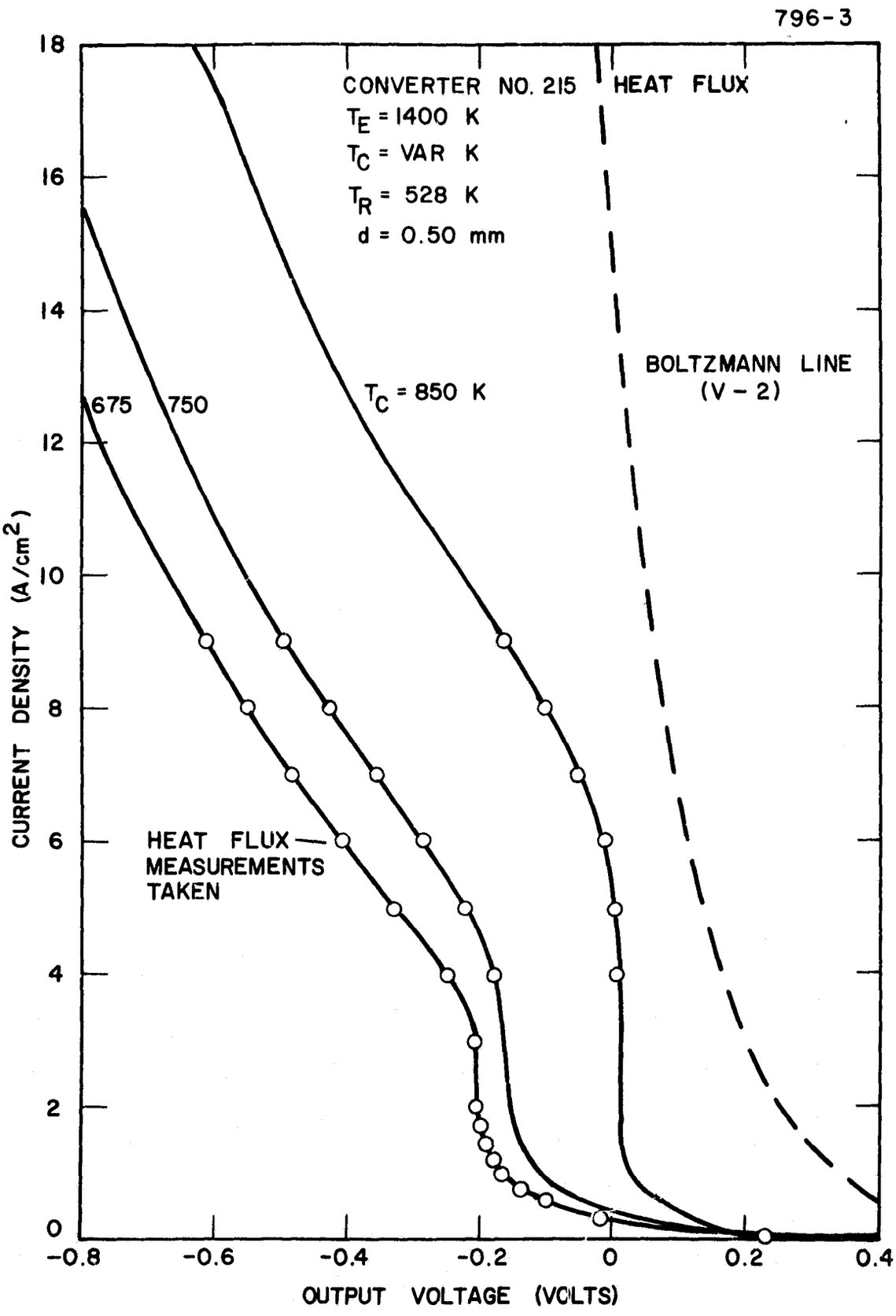


Figure 18. Collector Family for Converter No. 215

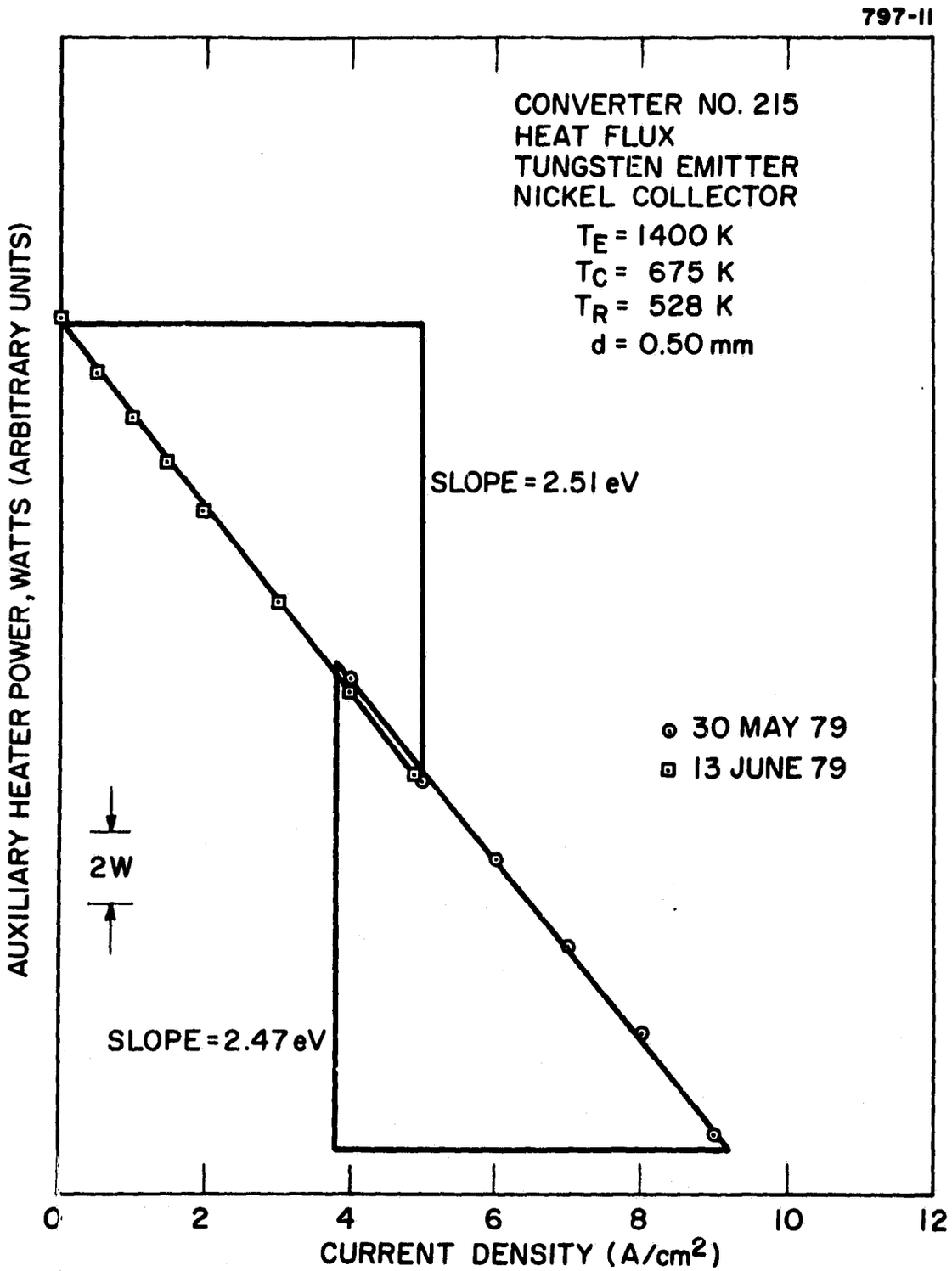


Figure 19. Heat Flux Data at $T_C$ = 675 K

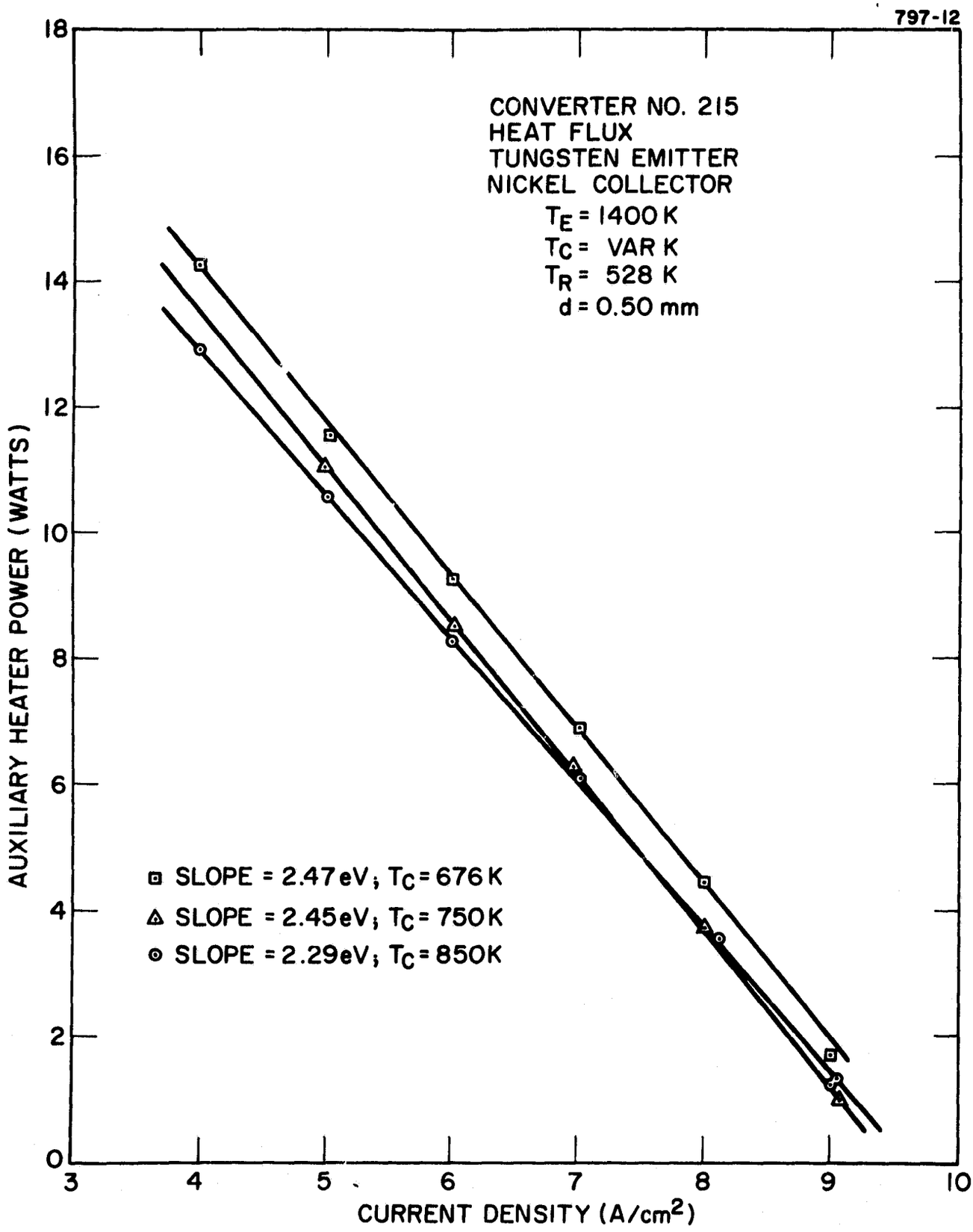


Figure 20. Heat Flux Data at Various Collector Temperatures

for $T_C$ = 750 K, and 2.47 eV for $T_C$ = 675 K. These results are plotted against collector work function and current-voltage offset (see Figure 18) in Figure 21. As shown in this figure, there is a good correlation between heat production at the collector and current-voltage offset.

Testing of the heat flux converter will continue during the next reporting period.

## III. COMPONENT HARDWARE DEVELOPMENT

### A. ALLOY HOT SHELL DEVELOPMENT

The testing of alloy hot shells in the Simulated Furnace has been resumed. In this furnace, the domes of the hot shells are exposed to products of combustion of a liquid hydrocarbon at 1200 C. The interiors of the shells are evacuated by an ion pump. The furnace temperature and the interior vacuum of each shell are recorded on a strip chart recorder. The accumulated test hours on the specimens are shown in Table II.

### B. CVD HOT SHELL-EMITTER DEVELOPMENT

Six leak tight composite hot shells, one inch in diameter, were fabricated during this reporting period.

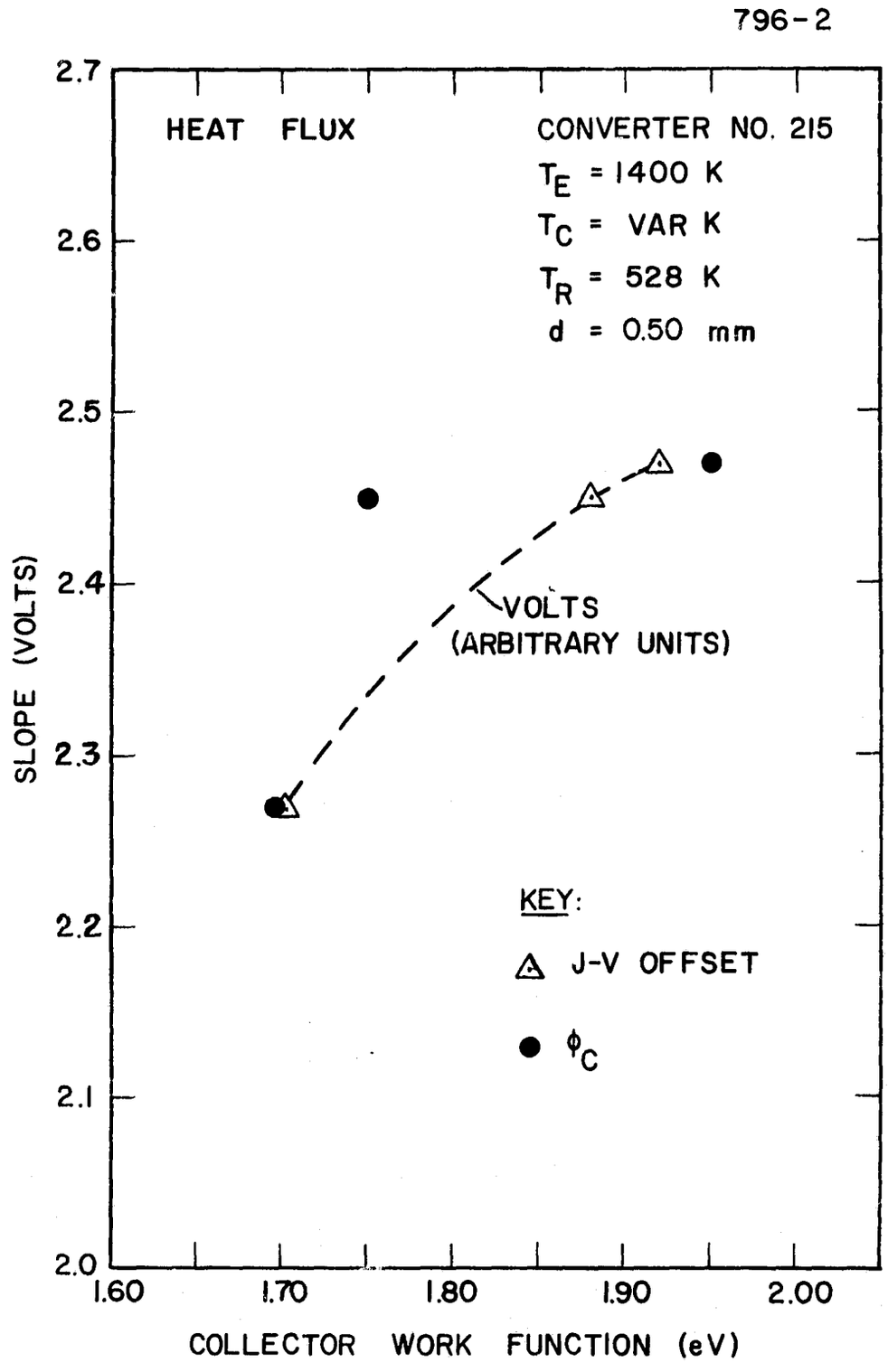


Figure 21. Heat Production at the Collector Versus Collector Work Function and Current-Voltage Offset

TABLE II

SIMULATED FURNACE TESTS
(9 July 1979)

| Test Port No. | Hot Shell | Test Hours | Comments | Date of Initiation |
|---|---|---|---|---|
| 1 | 446 CRES Cr-Ni Slurry Sinter | 705 | Leaktight | 20 Nov 1978 |
| 3 | 446 CRES Plasma Arc Sprayed with | 6179 | Leaktight | 31 Oct 1977 |
| 5 | 446 CRES Plasma Arc Sprayed with Nichrome | 6179 | Leaktight | 31 Oct 1977 |
| 6 | INCONEL 671 | 400 | Leaktight | 8 Mar 1979 |

Clock Reference 23183

Also, shells were produced under identical run conditons. One composite hot shell two inches in diameter was fabricated. In addition, three CVD tungsten deposits were made on arc-cast tungsten emitters for Auger and crystal orientation studies.

During this reporting period, two changes were made to the silicon carbide CVD procedure.

- Methane gas was omitted from the reaction.
- Graphite concentrators were polished and outgassed.

This improved procedure resulted in reduced nodules on the silicon carbide deposit and increased the percentage of leak tight deposits. All leak tight shells had the same interface geometry (see Figure 22), which required no machining for flange brazing.

A graphite mandrel two inches in diameter and four inches in length was coated on the inside with leak tight tungsten. The outer silicon carbide deposit was, however, not leak tight. Apparently this leak in the hemispherical part of the shell was caused by insufficient R.F. power to heat this larger area to the proper deposition temperature. In the future, the length of these shells should not exceed three inches. This will

allow the R.F. power available to heat the shell to a uniform and proper deposition temperature.

## IV. SYSTEM STUDIES

Stone and Webster Engineering Corporation has completed their preliminary study of a thermionic-topped central station powerplant fired with coal. A portion of the draft copy of the topical report summarizing the study has been received.

## V. TAM MODULE DEVELOPMENT

### A. CONVERTER NO. 218: CVD SILICON CARBIDE CONVERTER NO. 1

This flame-fired converter was constructed with a composite CVD hot shell-emitter (silicon carbide graphite tungsten). A cutaway drawing of the converter is shown in Figure 23. The emitter is approximately 100 mm in length and 25 mm in diameter. The dome is the active region of the hot shell-emitter and has an area of approximately 6 $cm^2$. The collector is made of nickel and is air cooled. The spacing between the collector and emitter is 0.2 mm at operating temperature.

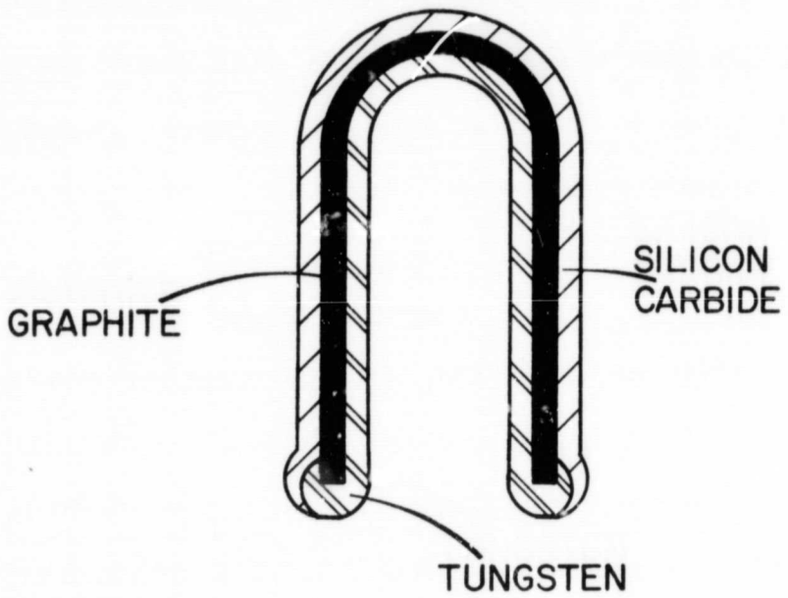


Figure 22. Cross Section of Hot Shell

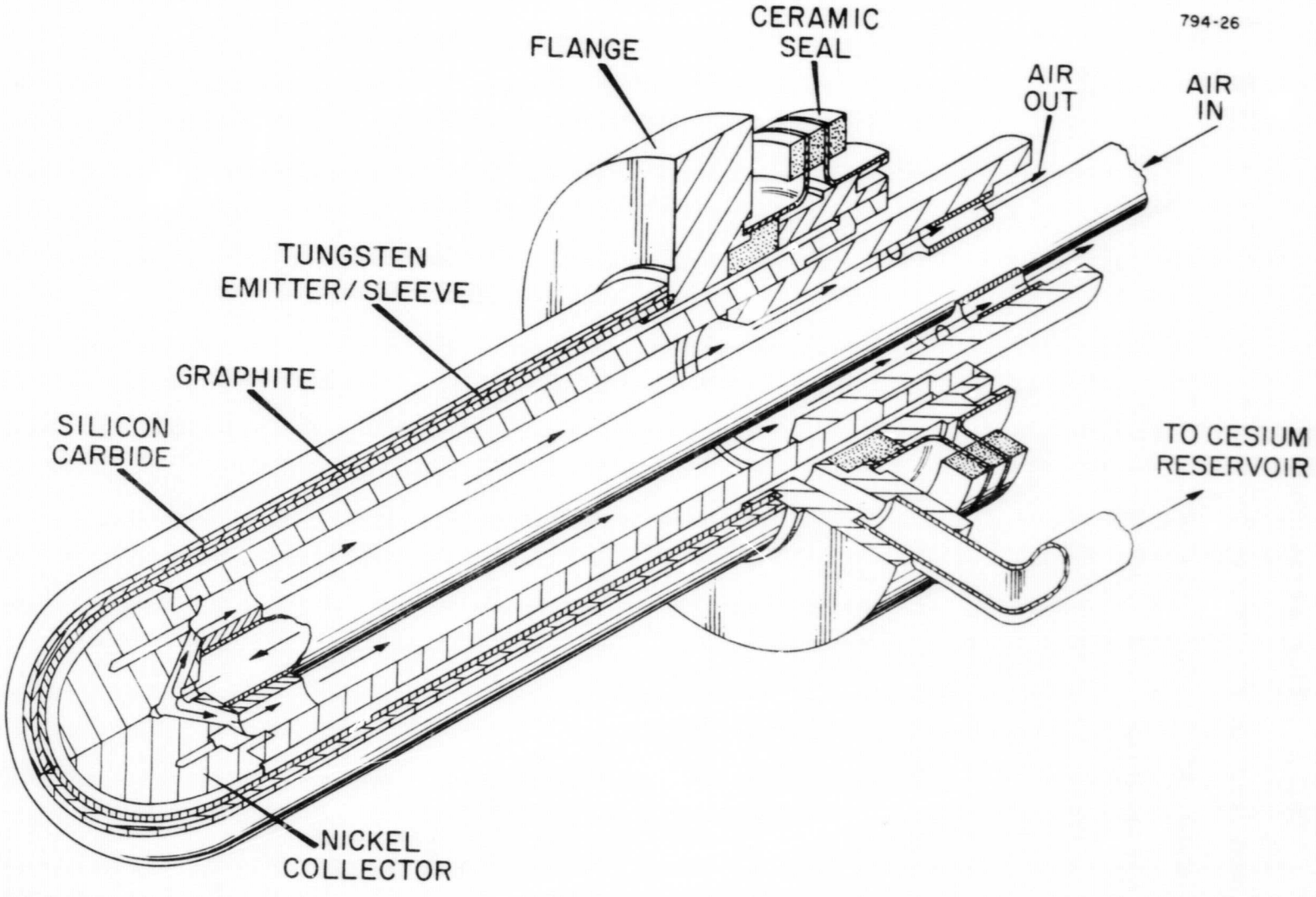


Figure 23. Flame Fired Converter With Composite CVD Hot Shell-Emitter (Silicon Carbide-Graphite-Tungsten)

The mounting arrangement of the CVD silicon carbide converter in the Multi-Converter Test Furnace is given in Figure 24. The mounting flange allows for simple installation and removal from the furnace of fully instrumented converters. The flange also supplies air cooling for the converter flange and mechanical support for the large current leads. The converter and mounting flange are installed in the bottom of the Multi-Converter Test Furnace shown in Figure 25. This facility uses from one to six natural gas-fired, flat, flame burners with recuperators.

The converter was outgassed to an emitter temperature of 1600 K with a pressure of less than $5 \times 10^{-8}$ torr. After outgassing, the furnace was cooled to room temperature and cesium was then distilled into the reservoir. Performance data were taken as the furnace slowly heated up. The emitter temperature ranged from 1600 to 1850 K. Figures 26 through 29 show typical current-voltage characteristics. Performance is optimized for all but the 1850 K case. The barrier index was 2.1 eV for optimized collector and cesium reservoir temperatures. The output power density was 4.5 $W/cm^2$

795-57

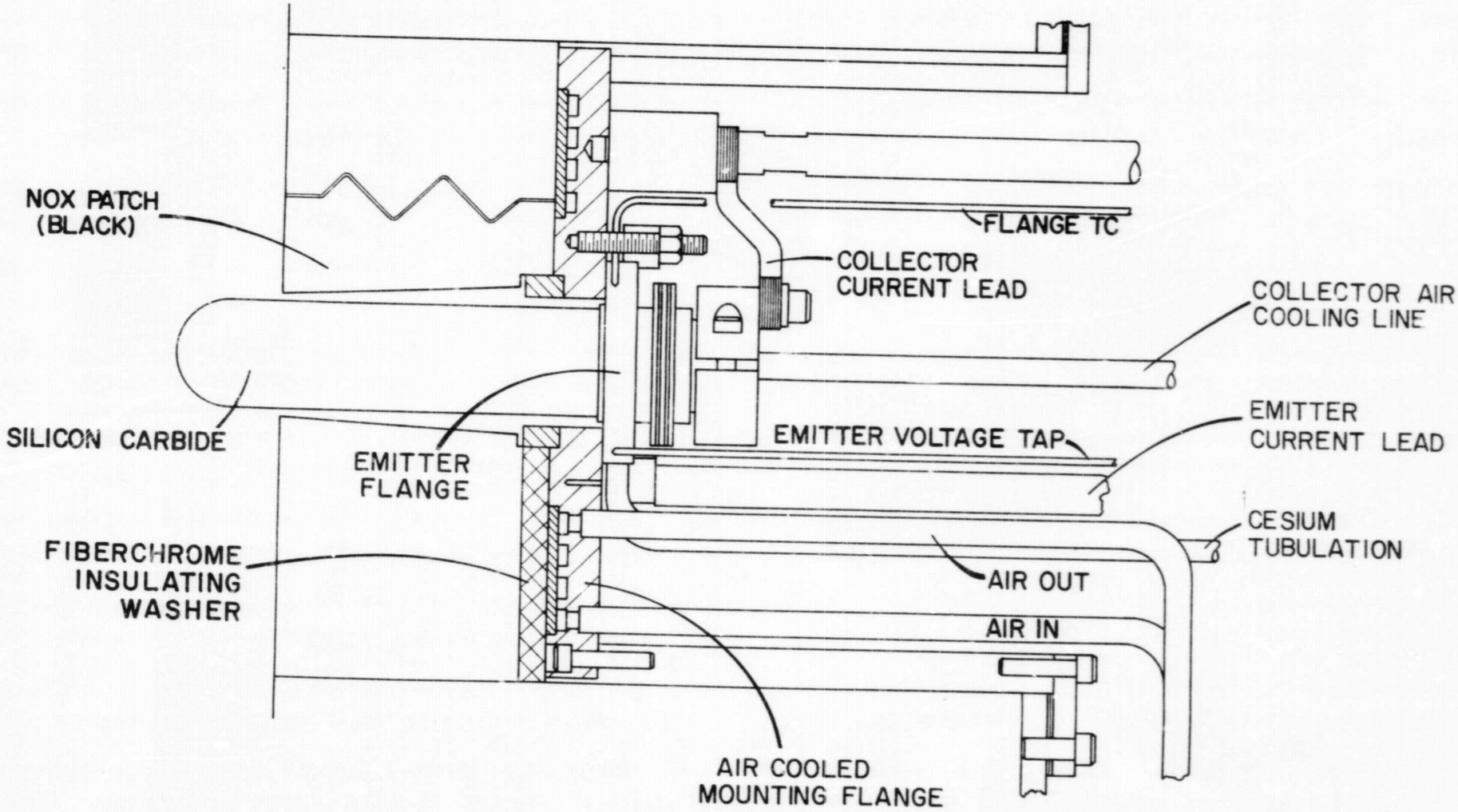


Figure 24. Detail of Mounting Flange

795-75

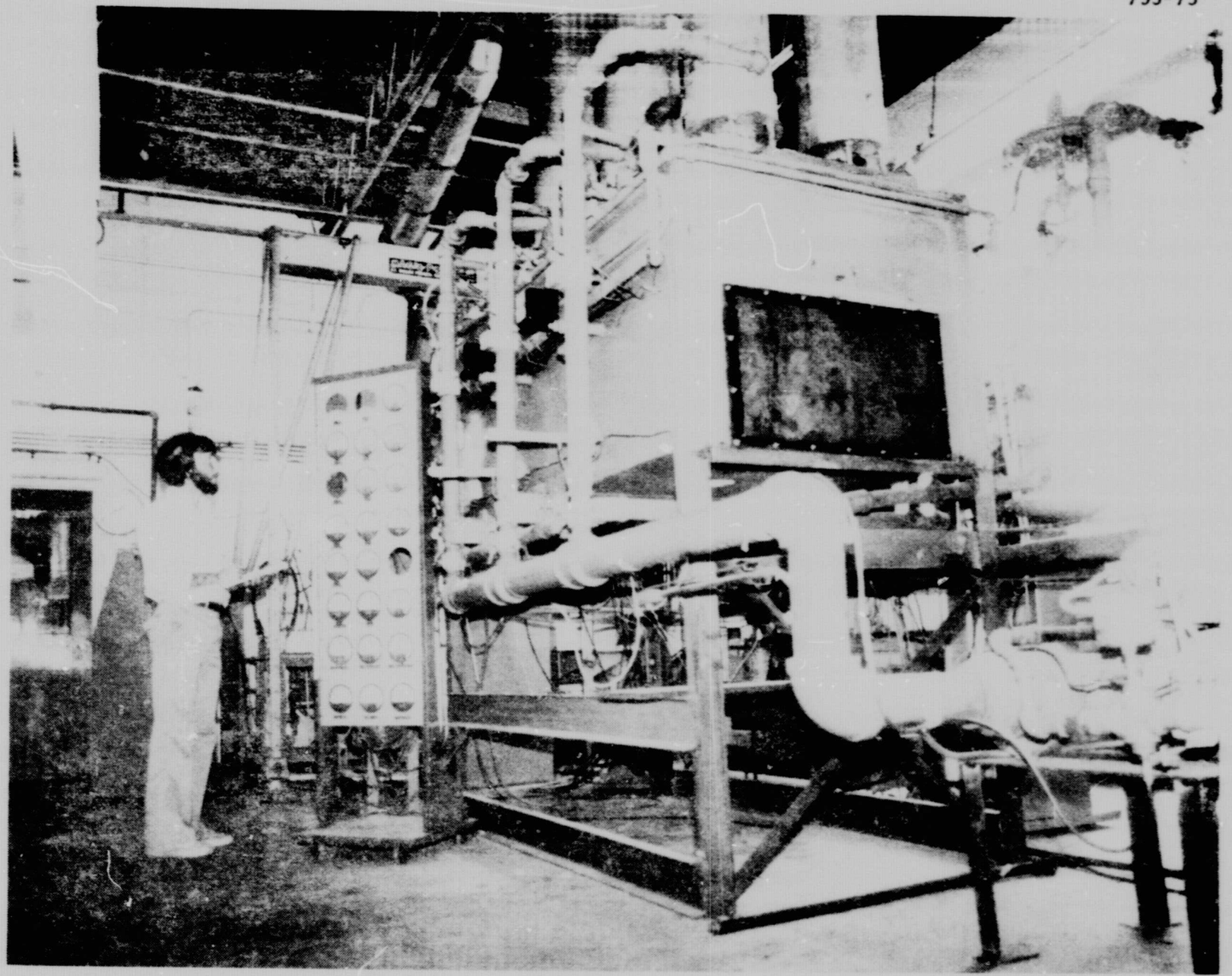

Figure 25. Multi-Converter Test Stand

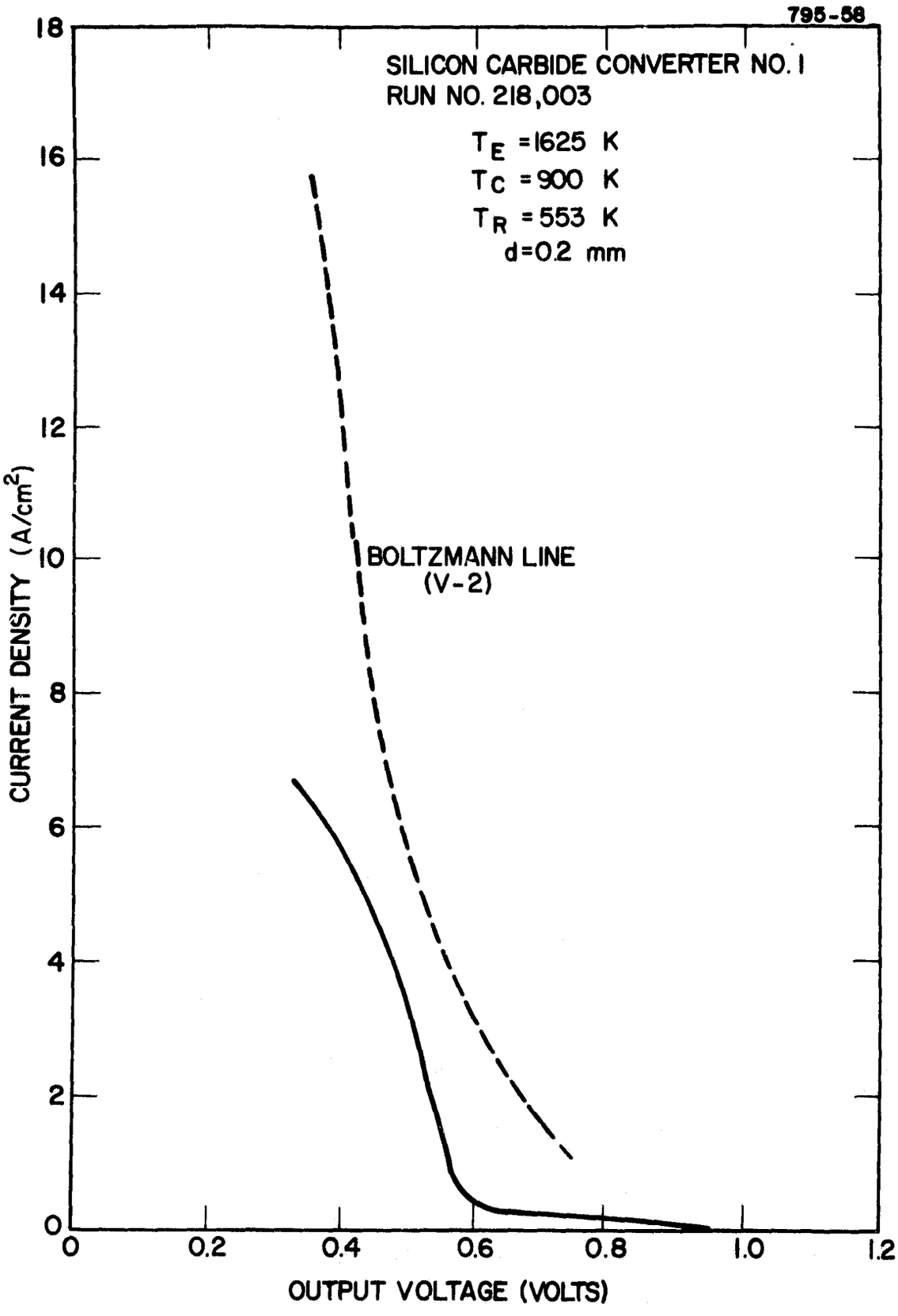


Figure 26. Current-Voltage Characteristic at an Emitter Temperature of 1625 K

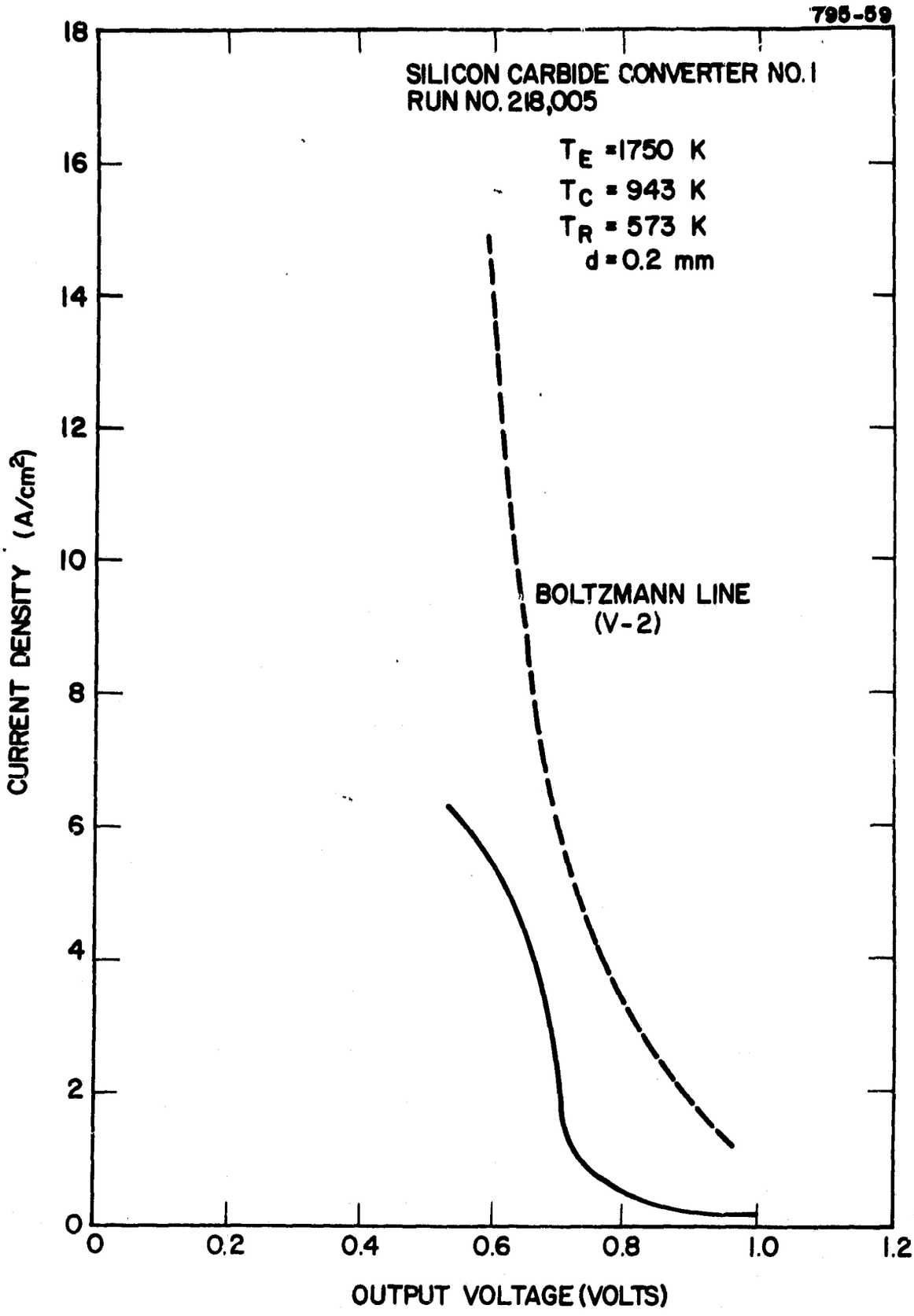


Figure 27. Current-Voltage Characteristic at an Emitter Temperature of 1750 K

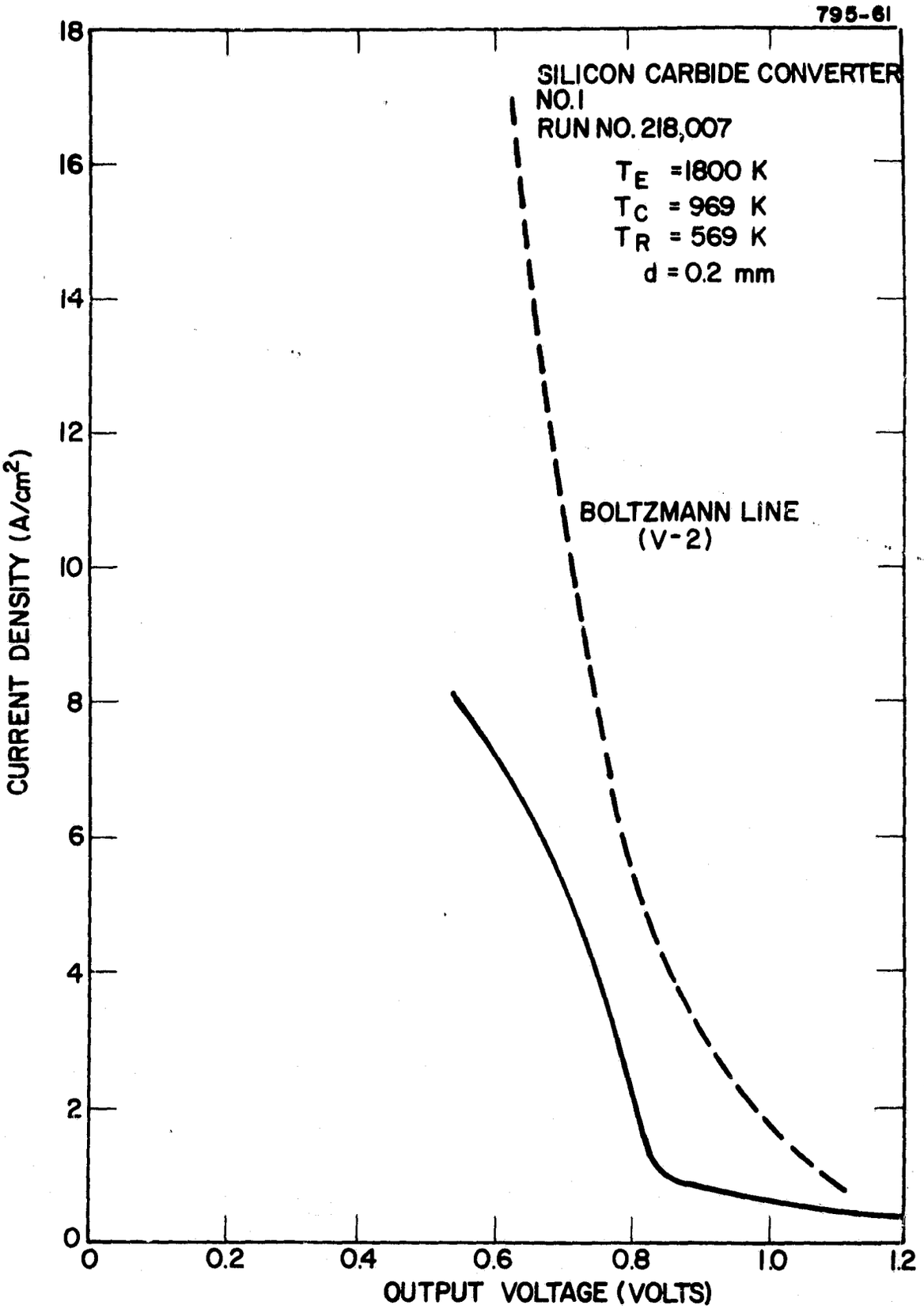


Figure 28. Current-Voltage Characteristic at an Emitter Temperature of 1800 K

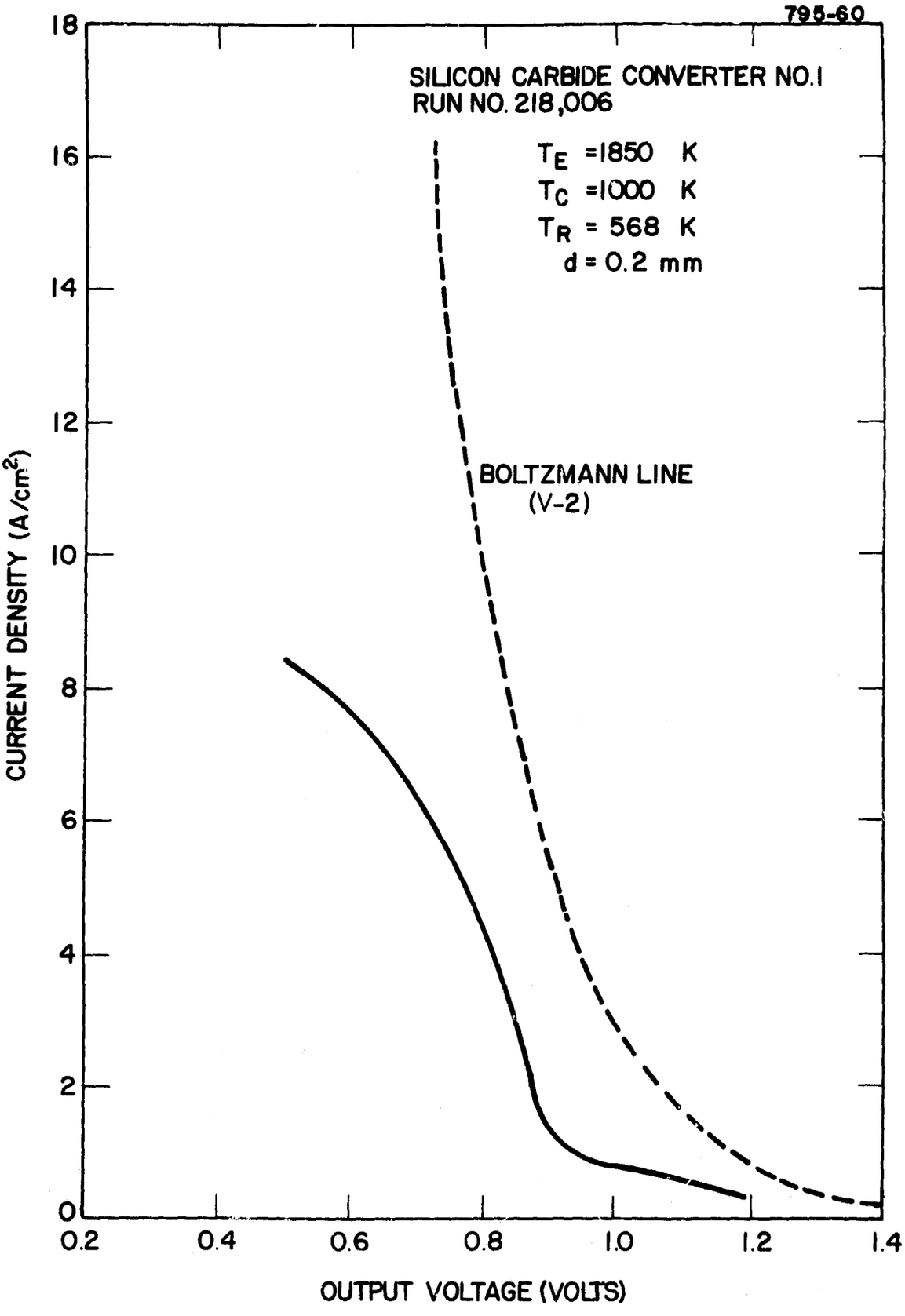


Figure 29. Current-Voltage Characteristic at an Emitter Temperature of 1850 K

at an emitter temperature of 1800 K. After performance data were taken at 1850 K the furnace was cooled and the life test of the converter was begun. The emitter temperature and output power density of the converter as a function of operating time is shown in Figure 30.

After 705 hours of operation the furnace was shut-down for maintenance.

After removing one side of the furnace wall to expose the converter, it was discovered that a steel pipe inside the furnace flue had melted and flowed onto the hot shell of the converter. Apparently, the converter suffered no ill effects from this exposure. When the furnace is restarted the maximum emitter temperature will be held to 1600 K to avoid remelting of the flue pipe. Several improvements in both the furnace and the converter mounting flange are being made during the shut-down.

## B. CONVERTER NO. 221: CVD SILICON CARBIDE CONVERTER NO. 2

A second CVD silicon carbide converter, essentially identical to the first, has been constructed. It will be installed in the Multi-Converter Test Furnace before it is restarted.

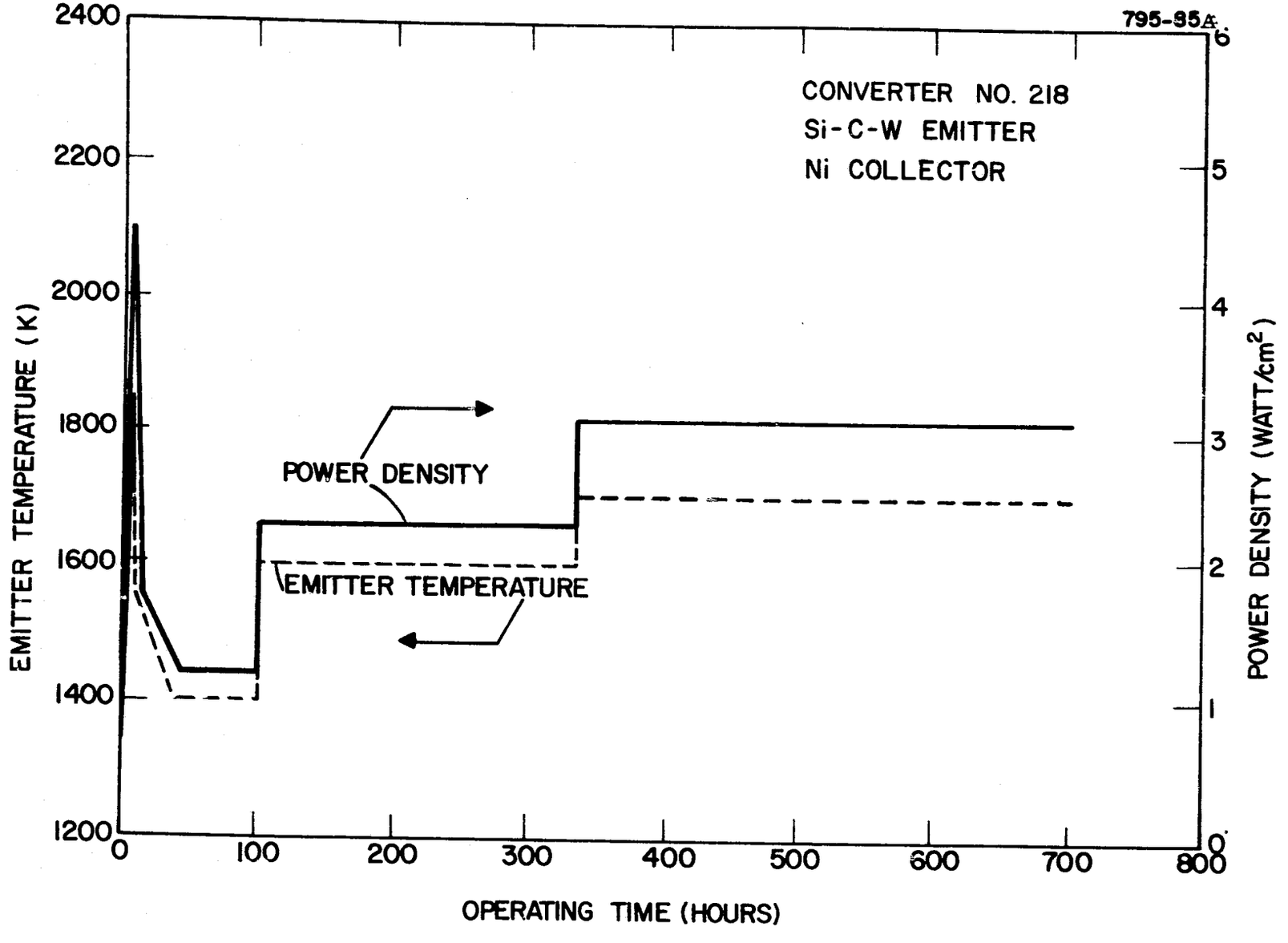


Figure 30. Emitter Temperature and Output Power Density as a Function of Operating Time

# PART TWO: JPL TASKS

## I. HIGH-TEMPERATURE CONVERTER EVALUATION

### A. CONVERTER NO. 216: TUNGSTEN EMITTER, MOLYBDENUM OXIDE COLLECTOR

After cesiation, an electrical short occurred in this converter. The short was persistent at spacings as wide as 1.5 mm, making testing of the converter impossible. Subsequently, the converter was disassembled. Visual inspection showed small pieces of metal flaking off the outer part of the collector body which faces the spacing pads on the emitter flange. This flaking metal was probably oxygenated molybdenum which was deposited during sublimation of the collector . The temperature of this surface during sublimation was probably not sufficiently high to provide adequate adhesion. In the future, any extraneous coatings will be removed prior to converter assembly.

Depcsitions on sandblasted and chemically etched surfaces show pronounced differences. Figure 31 shows two sublimed surfaces produced at the same time. Oxygen

797-13

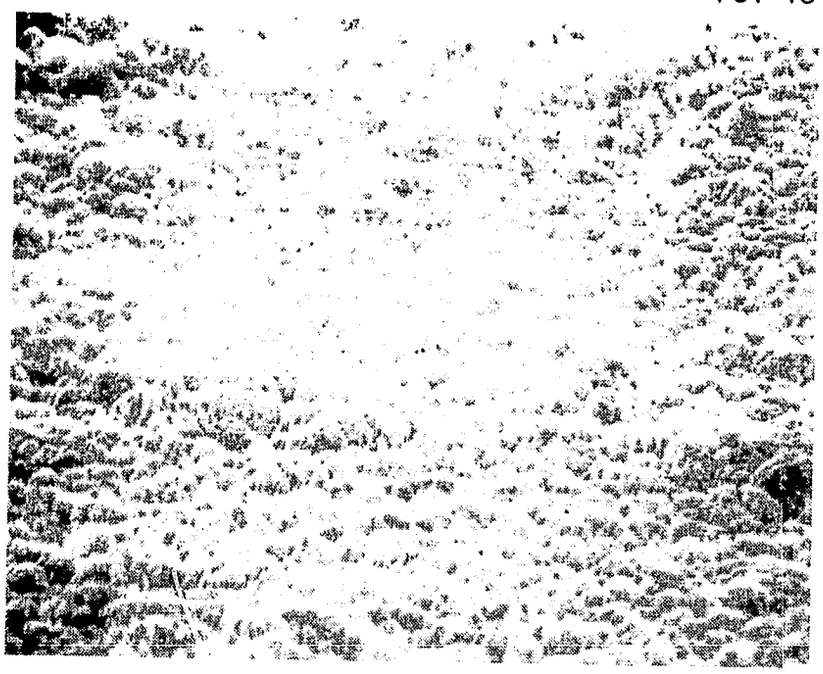

V-19A

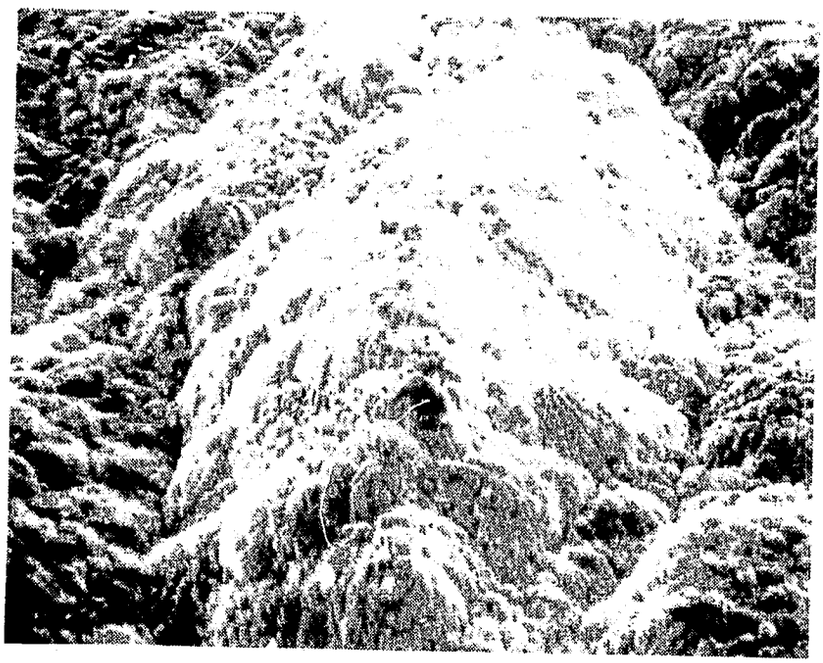

V-20A

Figure 31. Comparison of Deposits from Sublimed Molybdenum in Oxygen on Etched and Sandblasted Surfaces (2000 x)

contents for samples V-19A and V-20A were 1920 and 1980 ppm by weight, respectively. Sample V19-A was etched in a solution of hydrofluoric, nitric and sulfuric acids. Sample V-20A was sandblasted prior to sublimation. The chemically etched surfaces exhibited much smoother and more regular surfaces than the sandblasted surfaces. The similar oxygen concentrations of both surfaces indicate that the new sublimation furnace is yielding consistent results. A third surface (with a chemically etched substrate), prepared at the same time as V-19A and V-20A, is being fabricated into a converter (JPL No. 3).

## B. JPL CONVERTER NO. 7: Zr-O-W(100) EMITTER, NIOBOIM COLLECTOR

The fabrication of a Zr-O-W(100) emitter for JPL Converter No. 7 has been initiated. A W(100) surface was chemically vapor deposited from tungsten hexafluoride. A photomicrograph of a cross section of the deposition showing the 0.25 - 0.50 mm long single crystal columns is shown in Figure 32. X-ray analysis of the polished surface showed only the (100) peak, indicating a well-ordered surface. This polished surface will be dosed with zirconium and oxygen in the Surface Characterization

795-105

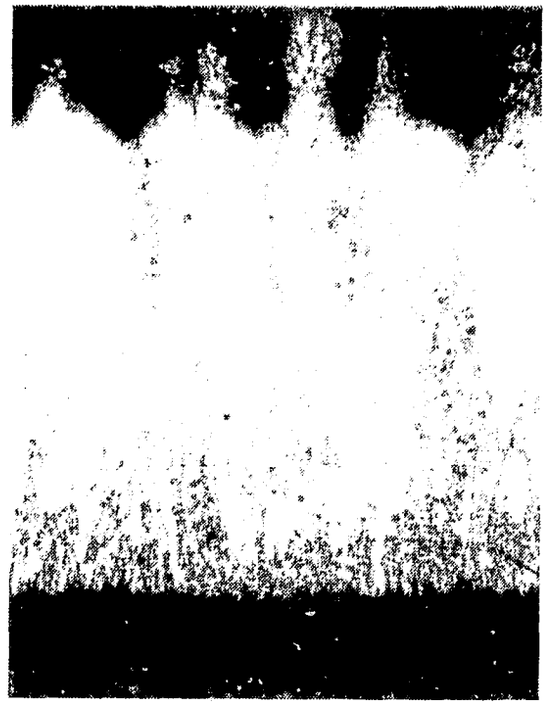

Figure 32. Photomicrograph of CVD Fluoride Tungsten Deposited at Thermo Electron Showing Columnar Structure. X-ray of Polished Surface Shows Only (100) Structure as Required for W-O-Zr Emitter.

Chamber to obtain a low work function emitter that requires little, or no, cesium. Bell-jar experiments are being performed to optimize the zirconium source geometry for uniform deposition.

## II. ADVANCED CONVERTER STUDIES

A bell-jar particle thermionic converter (PTC) and a cesiated PTC (Converter No. 220) were tested during this reporting period. The bell-jar PTC consisted of two "RCA nickel" electrodes sprayed with 1/2-mil coatings of "RCA barium oxide" (a composition of barium, strontium and calcuim oxides). This device was tested in a high vacuum ion pump system. The cesiated particle diode was tested in a conventional, variable-spacing, research converter. The emitter was molybdenum and the collector was 201 nickel. Both electrodes were sprayed with 1/2 mil coatings of BaO.

### A. NON-CESIATED PARTICLE THERMIONIC CONVERTER TEST

Activation of the RCA nickel electrode system was achieved by simultaneously heating the electrodes to 1323 K. Saturation currents measured at 973 K indicated an emitter work function of 1.67 eV and a collector work function of 1.61 eV. These values compare favorably with

the Nottingham work function relationship ( = 1.19 + 5 x $10^{-4}$ x T) and reflect a well-activated system. Current-voltage characteristics at emitter temperatures of 1173 K, 1273 K, and 1373 K were studied. Representative curves are shown in Figure 33. The collector in this device could be independently heated, but there was no mechanism for cooling the electrode. Consequently, for a specific emitter temperature, the collector could only be heated above its equilibrium temperature. Collector temperature families, such as those shown in Figure 34, indicate that lower collector temperatures would increase output.

A maximum output power of 60 $mW/cm^2$ was measured at an emitter temperature of 1373 K and a collector temperature of 1118 K. The short circuit current was 0.53 $A/cm^2$ and the open circuit voltage was 0.47 V. The output power was double that previously obtained in a PTC.

## B. CESIATED PARTICLE THERMIONIC CONVERTER TEST

During fabrication of this PTC (Converter No. 220) the sprayed emitter and collector surfaces were kept in contact. Prior to outgassing and activation the electrodes

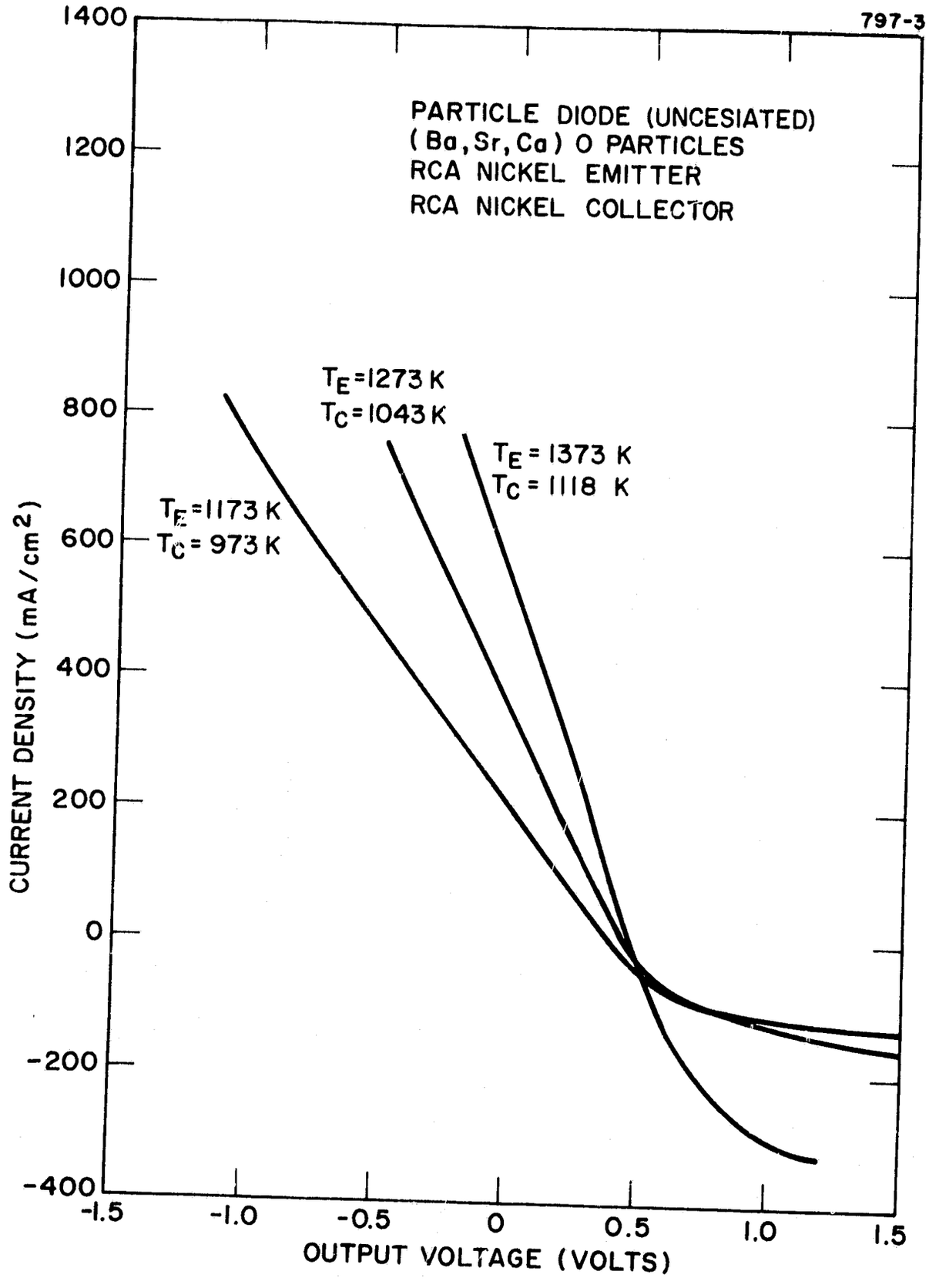


Figure 33. Output Characteristics of Bell Jar Particle Thermionic Converter No. 220

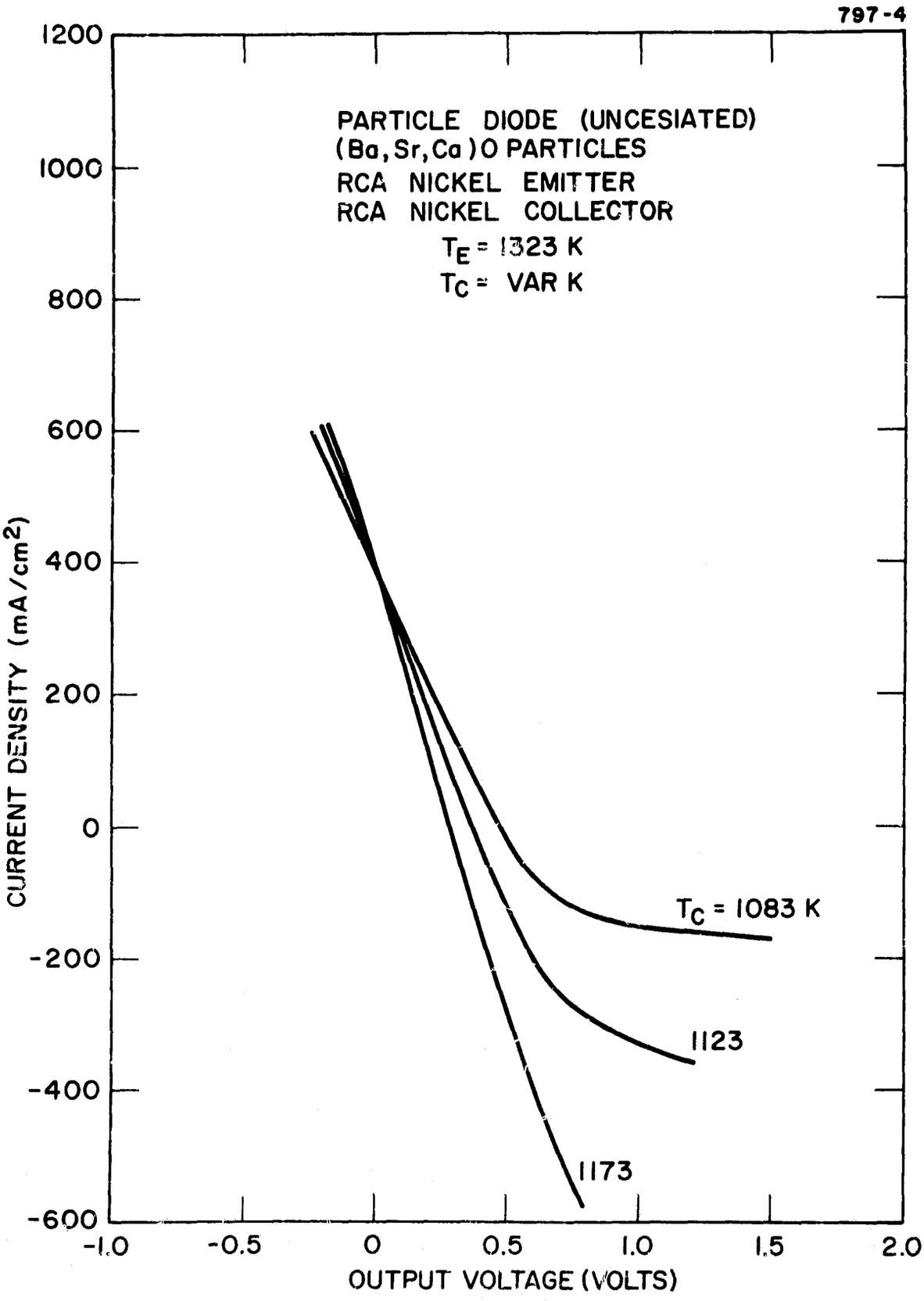


Figure 34. Current-Voltage Characteristics of Particle Thermionic Converter at Various Collector Temperatures, $T_E$ = 1323 K

were separated to a distance of 10 mils for a more complete outgassing of the sprayed coatings (evaporation of the nitrocellulose binder and conversion of the alkaline earth carbonates into BaO, SrO and CaO with the release of $CO_2$). After outgassing, the electrodes were activated.

The final work function values ($\phi_E$ = 1.95 eV and $\phi_C$ = 1.89 eV at 873 K) do not reflect a well-activated system (work functions around 1.63 eV at 873 K are expected). However, the emitter work function is consistent with previous BaO on molybdenum work function measurements (see Progress Report No. 38). The pressure obtainable in a research converter may also have negatively influenced the final activation states of the electrodes.

After activation the collector was lowered onto the emitter. The output characteristics indicated a partial short at $T_E$ = 1173 K, $T_C$ = 873 K. Despite repeated attempts to realign the electrodes (by adjusting the planetary gears of the spacing mechanism), the shorting could not be eliminated at these temperatures. Apparently, the problem was due to thermal expansion of the collector body, which stressed the coating. After the collector temperature was lowered to 673 K, the

leakage was reduced to an acceptable level. All subsequent current-voltage measurements were performed at this low collector temperature.

In the absence of cesium, the output of the diode at $T_E$ = 1173 K and $T_C$ = 673 K was quite low. The introduction of cesium caused a dramatic increase in output. A full cesium family for an emitter temperature of 1173 K is shown in Figure 35. Similar cesium families were studied at emitter temperatures of 1273 K and 1373 K. The performances of the PTC at these temperatures, with and without cesium, are given in Figure 36. Although specific curves did not reproduce well, a pronounced increase in output power with increasing cesium pressure was observed in all cases. Leakage in the converter increased as the data were acquired. The electrodes were separated and back-emission measurements were made at $T/T_R$ values ranging from 1.6 to 2.8 (see Figure 37).

## III. POSTOPERATIONAL DIAGNOSTICS

Auger analyses were performed for three converters after testing. Elemental compositions for Converter No. 210 (tungsten emitter, molybdenum oxide collector) are given in Table III. The circumferential area of the

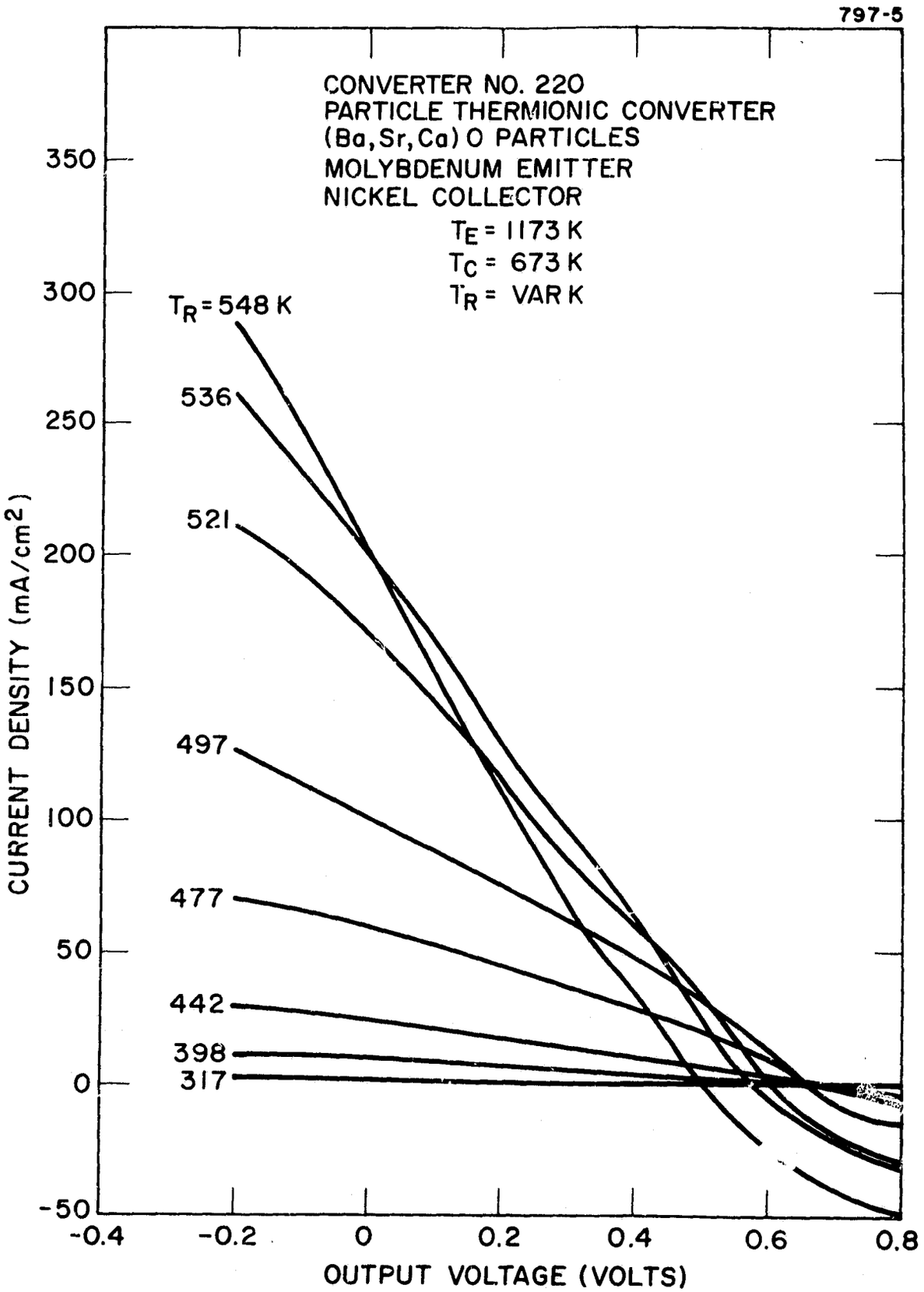


Figure 35. I-V Characteristics at Various Cesium Temperatures

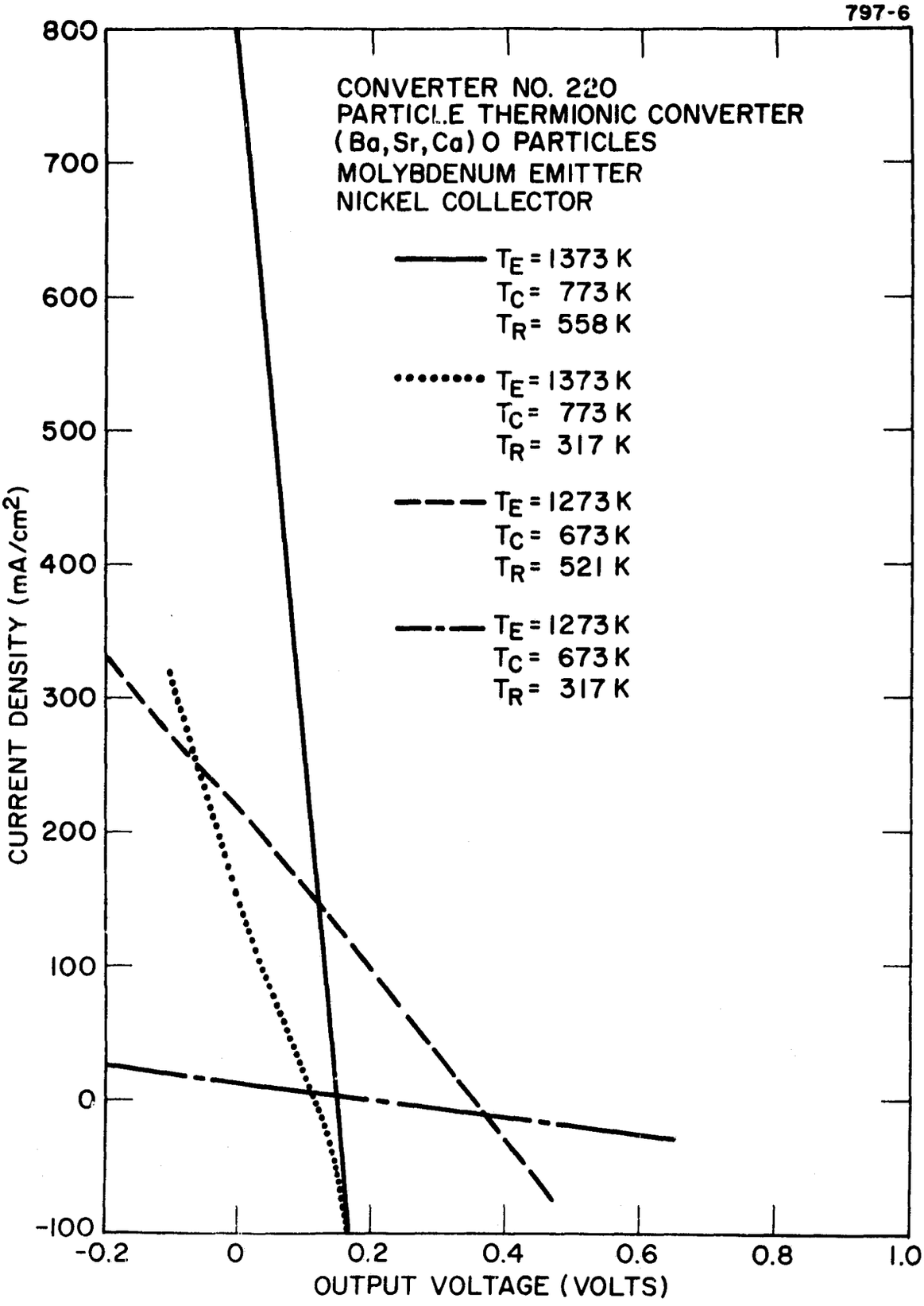


Figure 36. I-V Characteristics with and without Cesium, $T_E$ = 1273 K and 1373 K

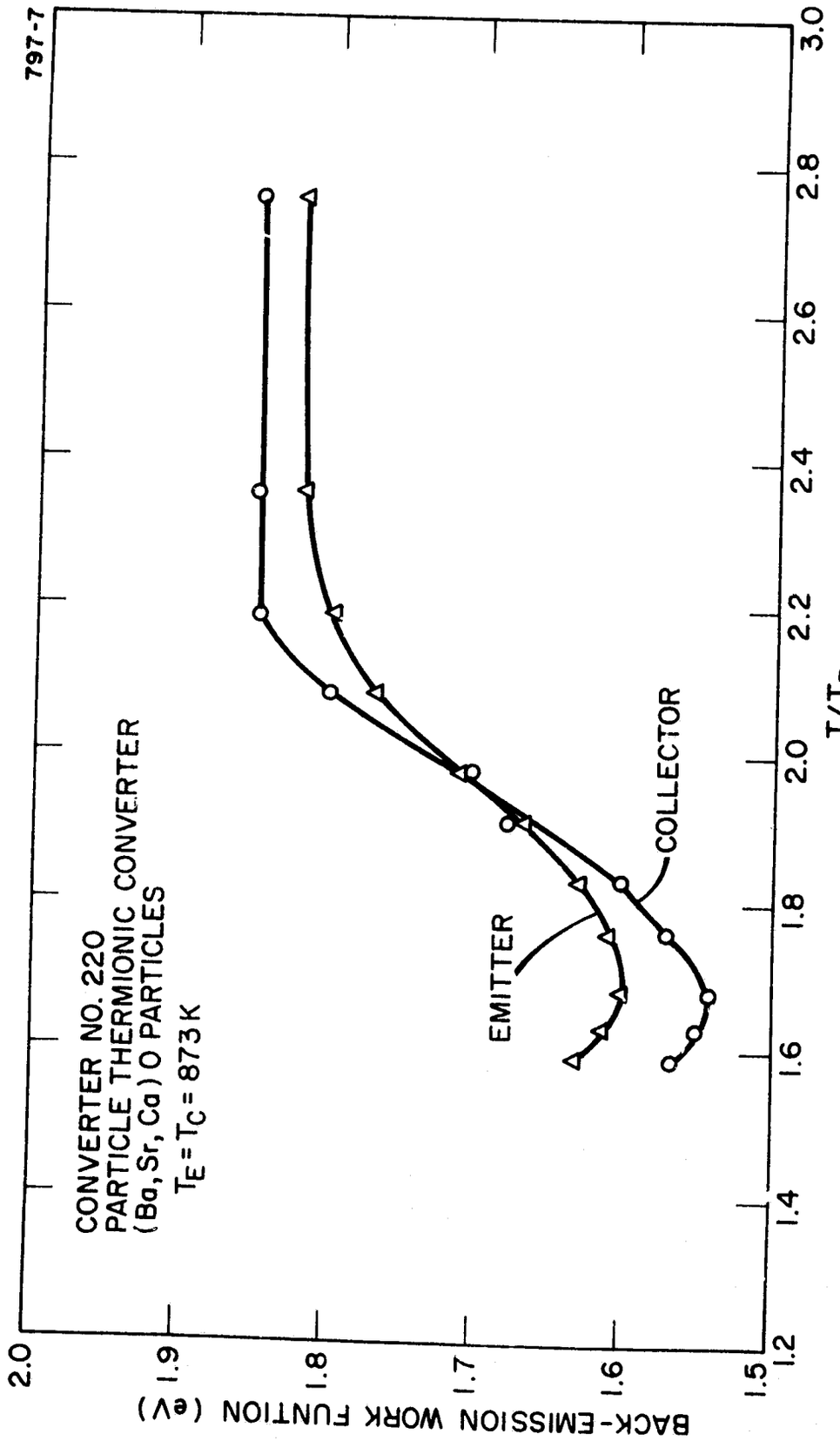


Figure 37. $T/T_R$ Plot for Emitter and Collector as Determined by Back-Emission Measurements

TABLE III
POSTOPERATIONAL AUGER ANALYSIS - CONVERTER NO. 210

| | EMITTER | | COLLECTOR | | |
|---|---|---|---|---|---|
| ELEMENT | OUTER AREA | CENTRAL WHITE REGION | OUTER AREA | CENTRAL WHITE REGION | DARK SPOTS |
| Mo | - | - | 2 | 2 | 2 |
| O | 10 | 6 | 17 | 17 | 35 |
| Cs | - | - | 33 | 26 | 17 |
| W | 34 | 18 | - | - | - |
| C | 53 | 72 | 18 | 26 | 10 |
| Na | 2 | 3 | - | - | - |
| Al | - | - | 6 | 28 | - |
| Si | - | - | 24 | - | 35 |
| S | 0.3 | - | - | - | - |
| Cl | - | 2 | - | - | - |

emitter contained tungsten and the usual carbon, oxygen, sodium, and sulfur impurities. The central portion of the emitter was white and contained somewhat more carbon and a small amount of chlorine. Some carbon probably diffused from the bulk during the long heating times at moderate temperatures. The balance of the carbon is probably due to atmospheric contamination. The collector had a central white region with a few dark-grey spots about 2 mm in diameter. The central white region consisted of primarily oxygen, cesium, carbon, and aluminum. Typically, the outside area and dark spots contained mostly oxygen, cesium, carbon, and silicon. The large amounts of aluminum and silicon on the collector are surprising. These elements probably reached the collector during the initial molybdenum oxide deposition, possibly from the hot insulators. Usually aluminum and silicon are present in much smaller amounts on converter electrodes.

Elemental compositions of Converter No. 214 ($LaB_{6.5}$ emitter, molybdenum collector) are given in Table IV. The compositions listed were taken at the centers of the electrodes, which were representative of the entire surface. After operation, the collector was

TABLE IV

POSTOPERATIONAL AUGER ANALYIS
CONVERTER NOS. 214 AND 196

| | CONVERTER NO. 214 ($LaB_{6.5}$/Molybdenum) | | CONVERTER NO. 196 (Triode) | |
|---|---|---|---|---|
| ELEMENT | EMITTER | COLLECTOR | EMITTER | WINDOW |
| B | 7 | 6 | - | - |
| La | 30 | 27 | - | - |
| C | 38 | 48 | 45 | 18 |
| O | 21 | 18 | 15 | 26 |
| Cs | 4 | - | - | 6 |
| Na | - | 0.4 | 5 | - |
| Al | - | 0.8 | - | - |
| N | 0.7 | - | 2 | - |
| Co | - | 0.3 | - | - |
| Ba | - | - | 5 | 49 |
| Cl | - | - | 1 | 2 |
| W | - | - | 28 | - |

reddish-purple in color and was covered with a fine white powder.

The white powder was probably a lanthanum oxide, since the analysis showed a large amount of lanthanum and oxygen on the collector. Some boron was also transferred from the emitter to the collector. The transfers of boron and lanthanum to the collector apparently occurred due to the formation of the volatile oxides $B_2O_3$ and LaO.

The compositions for the guarded collector triode (Converter No. 196) are also given in Table IV. The principal constituents of the emitter are carbon, tungsten, and oxygen. Although a small amount of barium is also present on the emitter, a much larger barium concentration appears on the window. This is reasonable since the barium from a dispenser-type cathode would be expected to eventually coat nearby cold surfaces.

## IV. CYLINDRICAL CONVERTER COMPONENT DEVELOPMENT

The machining of the cast sapphire tests components has been started. These components will be assembled and tested during the next reporting period.

Discussions have been held in regard to the "P" lead design with Mr. Valvo Roag of Syncal Corporation. He has supplied reference thermoelectric property data for future calculations. It has been decided that the initial "P" lead evaluation will use several legs rather than a cylindrical configuration.

## V. CORRELATION OF DESIGN INTERFACES

The design of the thermionic converter was updated to be consistent with the dimensions of the balance of the baseline system. This design is shown in Figure 38. The emitter diameter is 40 mm. It is bonded to the heat pipe by an insulating cermet. The wall thickness of the emitter is 3 mm and the effective emitter length is 160 mm, resulting in a converter length to diameter ratio of 4:1. The interelectrode gap is 1 mm and the collector wall thickness is 3 mm. The overall diameter of the collector heat pipe is 80 mm and it is electrically insulated from the collector heat pipe by a cermet or ceramic layer. An emitter semiconductor lead is also shown. An emitter-collector alumina insulator is provided at both ends of the converter.

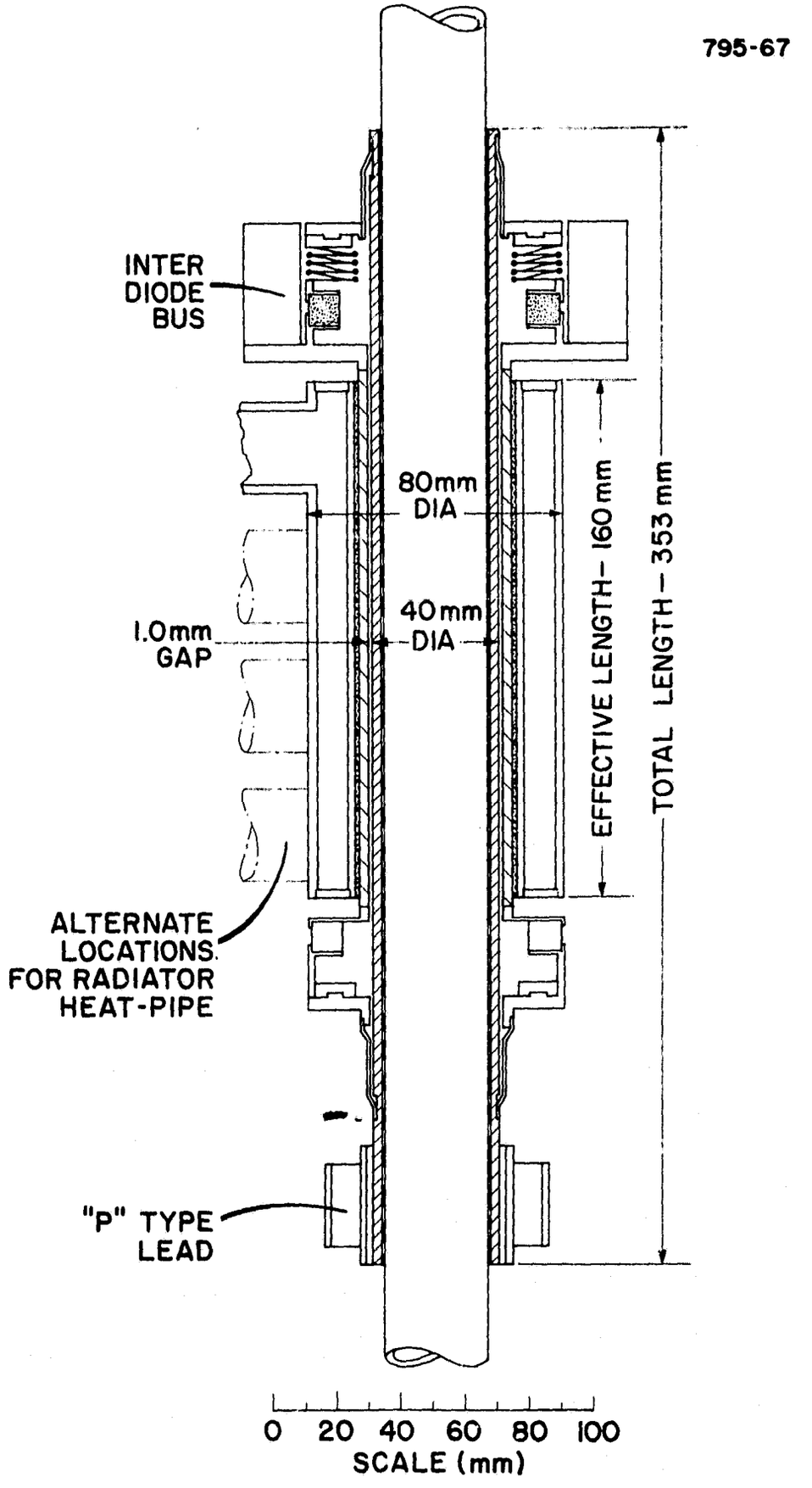


Figure 38. Thermionic Converter Design for Thermionic Reactor System

The collector and emitter structures are assembled separately. The collector structure is then assembled over the emitter and the emitter-to-collector heat chokes are magnetically swaged to the emitter before the final weld. Two collector structures are assembled to each emitter heat pipe. A bellows is provided at one end of the converter to allow for differential thermal expansion of the two electrode structures.

A design for connecting the converters was also developed. Heat is transported from the reactor to the conversion system via 200 emitter heat pipes. Each emitter heat pipe has two thermionic converters for a total of 400 converters. To achieve the desired redundancy, four converters are connected in parallel. The paralleled groups are then connected in series, as shown schematically in Figure 39A, to achieve the desired output voltage. An isometric view of the connection concept is shown in Figure 39B.

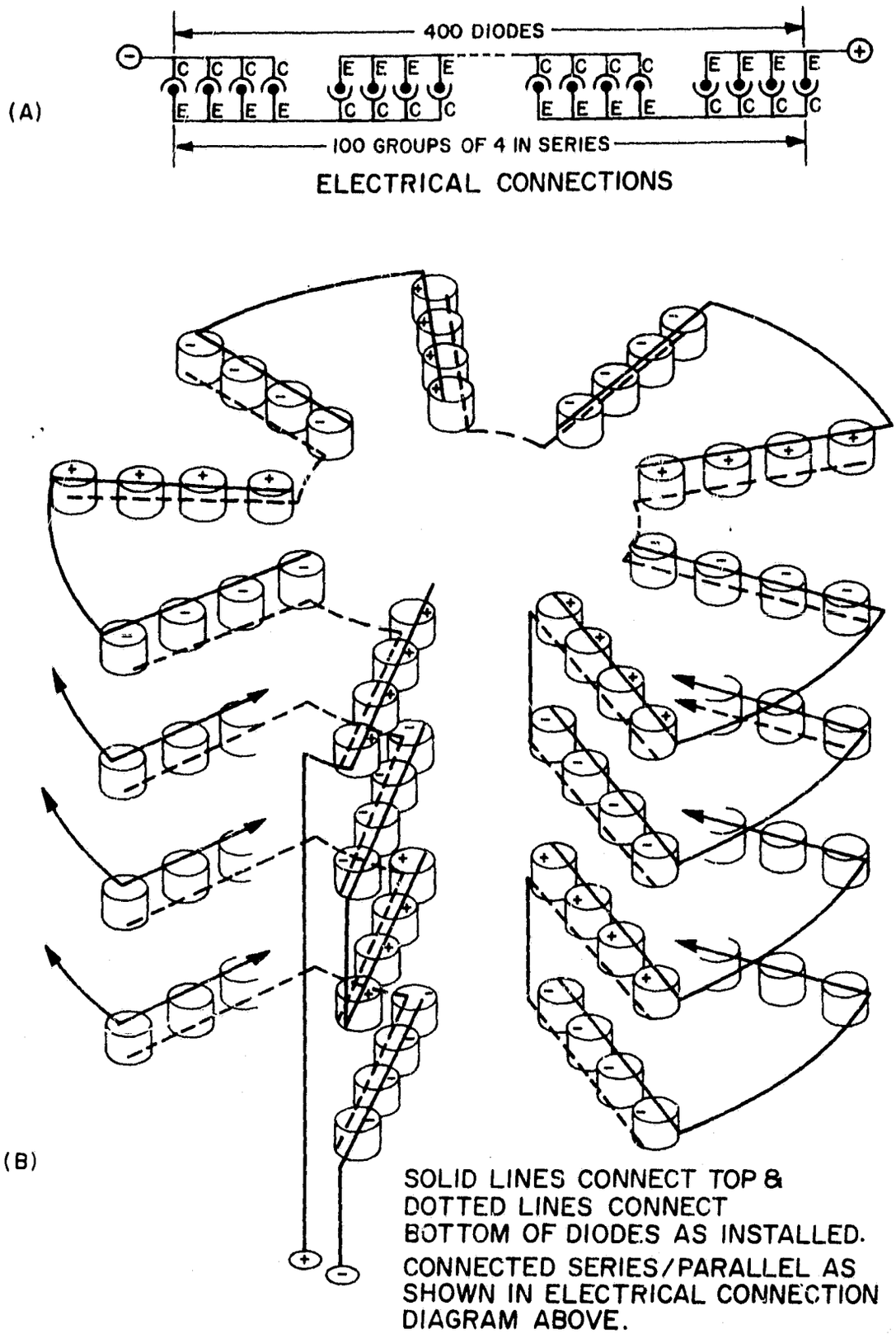


Figure 39. Design Approach to Connecting Thermionic Converters

## REFERENCES

1. Program Review Document, Thermo Electron Corp. Report No. TE 4258/4247-134-79 (June 1979).

2. G.A. Haas, A. Shih, R.E. Thomas, "Determination of Conduction Band Edge and Electron Affinity in Surface Potential Measurements of BaO," J. Appl. Phys. 47 (1976), p. 5400.

3. DOE/JPL Advanced Thermionic Technology Program Progress Report No. 36, Thermo Electron Corp. Report No. TE 4258/4247-57-79.

4. Wayne B. Nuttingham, Thermionic Emission, MIT Research Lab of Electronics, Technical Report No. 321 (Dec. 1956).

5. A.H. Sommer, T.R. Briere and F.N. Huffman, "Work Function Measurements of Cesium and Cesium-Oxygen Activated Surfaces," Proc. 1975 Thermionic Conversion Specialist Meeting, Einhoven, p. 43 (1975).

6. Thermophysical Properties Data Book, Thermophysical Properties Research Center, Purdue University.

7. DOE/JPL Advanced Thermionic Energy Conversion Joint Highlights and Status Report, Rasor Associates, (Nov. - Dec. 1978).